# HYDROGEN TERMINATED SILICON SURFACES: DEVELOPMENT OF SENSORS TO DETECT METALLIC CONTAMINANTS AND STABILITY STUDIES UNDER DIFFERENT ENVIRONMENTS

Thomas Anand Ponnuswamy, B.S., M.S.

Dissertation Prepared for the Degree of

DOCTOR OF PHILOSOPHY

UNIVERSITY OF NORTH TEXAS

August 2002

APPROVED:

Oliver M. R. Chyan, Major Professor
William E. Acree Jr., Committee Member
Martin Schwartz, Committee Member
Paul Marshall, Committee Member
Teresa Golden, Committee Member
Jeffery L. Coffer, External Committee Member
Ruthanne D. Thomas, Chair of the Department of Chemistry
C. Neal Tate, Dean of the Robert B. Toulouse School of Graduate Studies

Ponnuswamy, Thomas Anand, Hydrogen terminated silicon surfaces: Development of sensors to detect metallic contaminants and stability studies under different environments. Doctor of Philosophy (Analytical Chemistry), August 2002, 96 pp., 3 tables, 44 illustrations, reference list, 104 titles.

Hydrogen terminated silicon surfaces have been utilized to develop sensors for semiconductor and environmental applications. The interaction of these surfaces with different environments has also been studied in detail.

The sensor assembly relevant to the semiconductor industry utilizes a silicon-based sensor to detect trace levels of metallic contaminants in hydrofluoric acid. The sensor performance with respect to two non-contaminating reference electrode systems was evaluated. In the first case, conductive diamond was used as a reference electrode. In the second case, a dual silicon electrode system was used with one of the silicon-based electrodes protected with an anion permeable membrane behaving as the quasi reference electrode. Though both systems could function well as a suitable reference system, the dual silicon electrode design showed greater compatibility for the on-line detection of metallic impurities in HF etching baths. The silicon-based sensor assembly was able to detect parts- per-trillion to parts-per-billion levels of metal ion impurities in HF.

The sensor assembly developed for the environmental application makes use of a novel method for the detection of $Ni^{2+}$using attenuated total reflection (ATR) technique. The nickel infrared sensor was prepared on a silicon ATR crystal uniformly coated by a 1.5 micron Nafion film embedded with dimethylglyoxime (DMG) probe molecules. The detection of $Ni^{2+}$ was based on the appearance of a unique infrared absorption peak at

1572 $cm^{-1}$ that corresponds to the C=N stretching mode in the nickel dimethylglyoximate, $Ni(DMG)_{2,}$ complex. The suitable operational pH range for the nickel infrared sensor is between 6-8. The detection limit of the nickel infrared sensor is 1 ppm in the sample solution of pH=8.

ATR – FTIR spectroscopy was used to study the changes that the hydride mode underwent when subjected to different environments. The presence of trace amounts of $Cu^{2+}$ in HF solutions was found to roughen the silicon surface as observed by ATR-IR spectroscopy. The initial stages of oxidation in UPW and $Cu^{2+}$ / UPW was studied. Trace amounts of $Cu^{2+}$ were found to drastically increase the rate of oxidation, while the rate of oxidation was found to be retarded on removing dissolved oxygen that was present in UPW.

ACKNOWLEDGMENTS

I would like to thank my advisor Dr. Oliver M. R. Chyan for his guidance during the course of my research. I would also like to thank my wife and parents for their continual encouragement and support.

TABLE OF CONTENTS

LIST OF TABLES

LIST OF ILLUSTRATIONS

# CHAPTER 1

## INTRODUCTION

This chapter serves as an ideal platform to lay out the contents of this dissertation. As the title suggests, the focus of the research is on studying and utilizing the properties of silicon surfaces. Silicon, whether in single crystal or polycrystalline form, has received considerable attention due to its widespread use in the fabrication of electronic devices. In order to increase its conductivity, the Si atoms present in the lattice are substituted with other foreign atoms with different valencies and this phenomenon is termed as doping. For example, the doping of crystalline silicon with phosphorous leads to the replacement of tetravalent silicon atoms from the lattice with that of pentavalent phosphorus atoms resulting in the formation *n* type silicon substrates. The prefix *n* stands for negative and is attained due to the excess of electrons caused by the substitution process. On the other hand, doping with trivalent B results in the formation of *p* type silicon substrates, which indicates the presence of holes or positive charge in the crystal structure. As Chapter 2 and Chapter 4 are directly related to the semiconductor industry, it is worthwhile to understand the role of silicon in this large-scale industry.

More than 90% of the electronic devices are fabricated on IC's (Integrated circuits), which are based on silicon substrates. An IC is essentially a combination of resistors, diodes and transistors that are needed for the functioning of all electronic devices. The first IC was built in 1959 by Jack Kilby and was in fact made out of germanium. The shift to silicon occurred because of the inherent shortcomings of

germanium, namely, low melting point (937$^{o}$C) and its inability to form stable oxides.[1] Silicon on the other hand forms a very stable oxide, and is a key structure for microelectronic devices as will be seen later in the section. It also has a fairly high melting point of 1687 K, which is a major advantage as many of the processes involved in the fabrication of IC's involve fairly high temperatures.

### 1.1 Structure and working of MOSFET

MOSFET (Metal oxide semiconductor field emitting transistor) is the basic structure in all digital devices.[2] The MOSFET is a voltage-controlled device, wherein the input voltage is amplified.

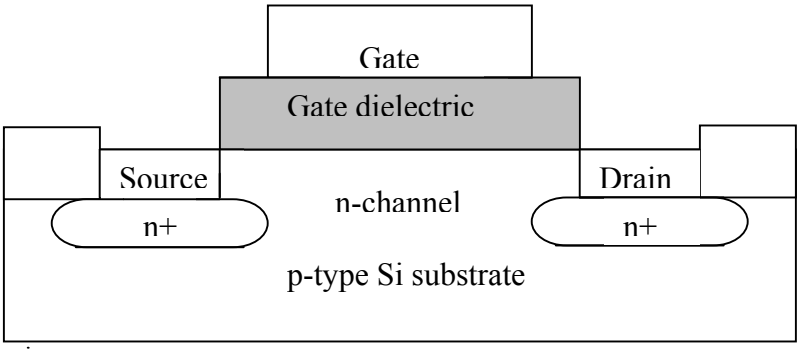


**Fig. 1.1** Structure of an *n* – channel MOSFET.

The base substrate of a *n* – channel MOSFET (Fig. 1.1) is a *p* type silicon which has localized n type regions formed with the help of ion implantation which are denoted a $n^{+}$ as they are electron rich regions and called the source and the drain. The region denoted as *'n -channel'* represents the channel through which the electrons flow between the source and the drain. A thin layer of $SiO_2$ (50 – 100nm) covers these n type regions and is

referred to as gate oxide. The gate material is normally doped polysilicon, which is deposited over the gate oxide. When a voltage (gate voltage) is applied to the gate and it is more than a certain threshold voltage, a field is generated in the surface of the silicon substrate resulting in a buildup or depletion of charges below the gate oxide depending on the polarity of the voltage. The source is biased with respect to the gate voltage and the drain is grounded relative to the source. This results in the flow of current between the source and drain, representing an 'on' state. The off state corresponds to the case when no current flows in the channel. The MOSFET can thus be considered as an on /off switch.

| **Contaminant** | **Source** | **Impact** |
|---|---|---|
| Sodium | DI water, chemicals | Gate oxide integrity |
| Aluminum | Chemicals | Gate oxide kinetics |
| Iron, copper, nickel | Chemicals | Minority carrier lifetime |
| Calcium | Chemicals | Surface roughness |
| Fluoride | HF, DI water | Gate oxide kinetics |
| Phosphate | Chemical | Gate oxide integrity |
| Ammonia | $NH_4OH$ | Haze |
| Sulfate | $H_2SO_4$ | Haze |
| Oxygen | DI water | Quality of film |
| Particle | Acids, DI water | Gate oxide integrity |
| Bacteria | DI water | Organic induced defects |
| Silica | DI water | Particle induced defects |

**Table 1.1.** Common contaminants generated during the cleaning process.[3]

The normal functioning of the MOSFET can be adversely affected by trace amounts of contaminants. The common contaminants are *particles, metallic ions, chemicals and bacteria*.[2] With the miniaturization of devices, the gate oxide thickness and channel length are decreasing at a very fast pace, thereby leading to the decrease in the threshold voltage. This decrease in the size of devices indicates that the tolerance specification for these contaminants becomes even tighter and contamination control becomes even more critical. One of the major contaminants is the presence of metallic ions, which has a deleterious effect on the reliability of devices. Some of the metallic contaminants have very high mobility in the silicon substrate and can change the electrical performance of the devices. The integrity of the oxides is also compromised due to the presence of these contaminants as the oxide then ceases to be a pure dielectric material. Thus on applying the required threshold voltage one would observe current leakage, which would lead to the failure of the device. Some of the common metallic contaminants are $Cu^{2+}$, $Au^{3+}$, $Ag^{+}$, $Ti^{4+}$, $Cr^{2+}$, $Ni^{2+}$, $Fe^{3+}$, $Na^{+}$, $K^{+}$ etc. They are known to exist in processing chemicals and in the surroundings of IC fabs.[2]

Chapter 2 deals with the development of a stable reference system to detect trace amounts of metallic contaminants using a silicon-based sensor. Chyan *et al.* have previously shown that silicon based potentiomentric sensors have the capacity to detect ppb – ppt levels of metallic contaminants.[4] The disadvantage in that approach was caused due to the usage of Ag /AgCl reference electrode which tends to effuse $Ag^{+}$ into the analyte thereby contaminating the solution under analysis. Though, Chapter 2 deals with developing an online monitoring method for metallic contaminants in semiconductor

based chemicals, the focus is on developing an ideal reference electrode capable of matching up to this task.

Chapter 3 deals with the development of a novel silicon based sensor for detecting $Ni^{2+}$ in the environment. To my best knowledge this is the first time that the detection of $Ni^{2+}$ using ATR – IR spectroscopy (Attenuated total reflection) has been reported. The development and characterization of the sensor will be dealt in detail in that chapter.

Chapter 4 is a study of hydrogen terminated Si(100) substrate under different environments. The goal of this study is to understand the reactions that have an impact on the hydrogen terminated state of silicon surfaces during its interaction with HF and ultrapure water (UPW) under various conditions. ATR – IR spectroscopy has been used for this purpose, as it is capable of giving detailed information of surface states with ease and the required resolution.

## 1.2 Structure of Single Crystal Silicon surfaces

This section deals with the basic structure of the most commonly used single crystal surfaces. The Si unit cell has a diamond like structure with each Si atom bonded to four others resulting in a tetrahedral structure. This arrangement corresponds to two interpenetrating fcc lattices with one being displaced ¼ of a lattice constant in each direction from the other.[5] Single crystal silicon substrates are used in the fabrication of microelectronic devices instead of polycrystalline substrates as they have a more uniform structure thereby making them more predictable in terms of their properties. Si (100) and (111) orientations are the two most commonly used structures in the semiconductor

industry. The (100) and (111) orientation correspond to the miller indices for a cubic crystal structure.

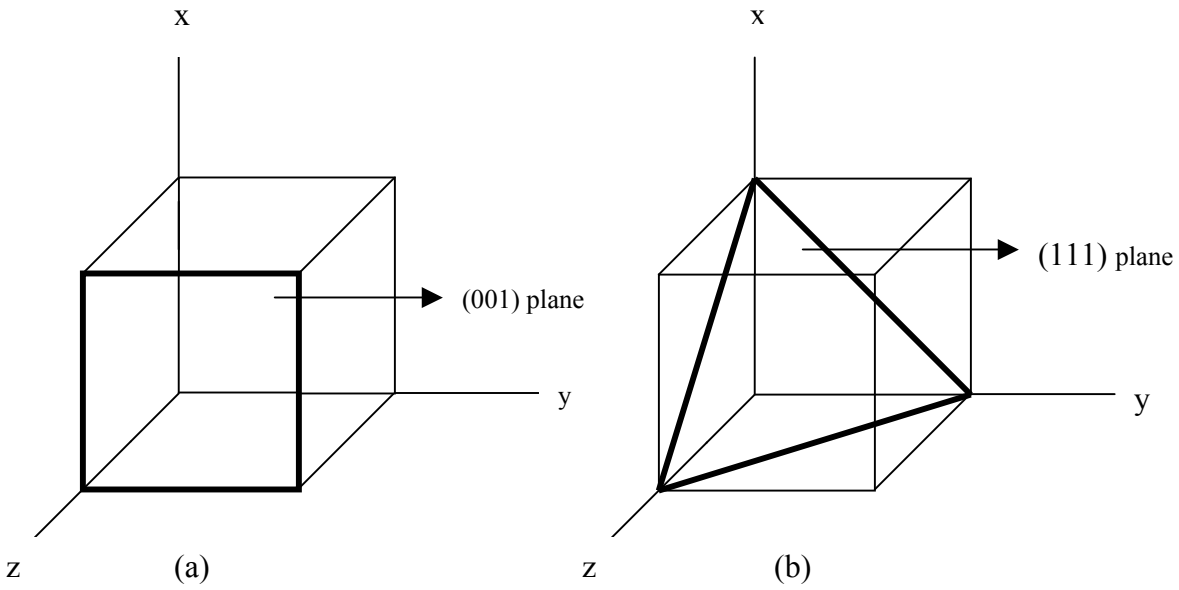


**Fig. 1.2.** Crystal structure representing (a) (100) orientation (b) (111) orientation.

Miller indices are the set of integers that describe a given plane in a crystal. They are the reciprocal of the intercept that is formed by the three axis of a cubic crystal system. In the case of (100) orientation the resulting plane of the unit cell is a square while in the case of (111) it is a triangle (Fig. 1.2). The slicing of single crystal silicon through a particular plane generates a substrate which has a specific plane exposed. Each of these planes is unique as they differ in atom count and binding energies between the atoms. These differences result in different physical, chemical and electrical properties. My research focuses on the Si(100) single crystal as majority of the devices are fabricated on such a substrate. A (100) orientation leads to a more open lattice structure, which is easy to cleave and etch chemically.

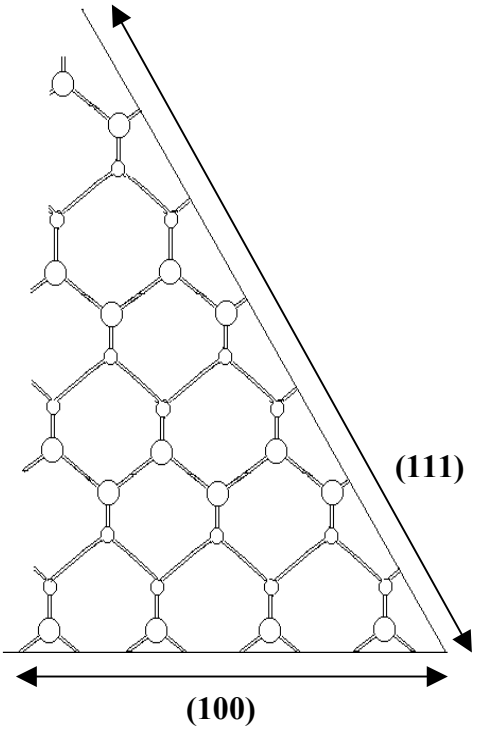


**Fig. 1.3.** Schematic representing the dangling bond formation for the (100) and (111)

The bulk structure of Si represents the tetrahedral arrangement of atoms (Fig. 1.3). The smaller circles represent atoms that are pointing away from the page. It can be clearly seen that the surface atoms for (111) and (100) orientation contain one and two dangling bonds respectively.

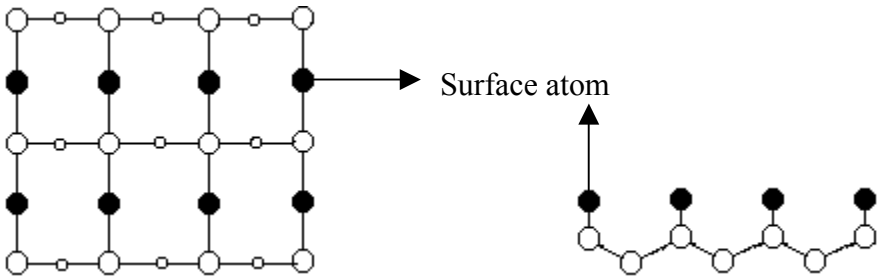


**Fig. 1.4.** Structure of Si(100) (a) Top view (b) Side view.

The Si(100) plane has a square lattice wherein each silicon atom is bonded to two atoms below its plane and two above. According to Fig. 1.4 the surface atom has two dangling bonds. The presence of these bonds renders the surface very reactive, which can be decreased by surface reconstruction or capping these bonds with foreign atoms.[6] The chemisorption of atomic hydrogen to the dangling bonds makes the surface very stable and prevents further reaction. This is in fact one of the main reasons for treating the silicon surface with HF as will be seen later.

### 1.3. Silicon Surface Preparation

The pre-treatment of the silicon surface is one of the essential steps needed to use it as a base for fabricating IC devices. The pre-treatments are discussed below, as they were used during the course of my research. The combination of all these cleans is referred to as the RCA (Radio Corporation of America) clean.[7]

| **Common Name** | **Composition** | **Purpose** |
|---|---|---|
| DHF | $HF + H_2O$ | Etching $SiO_2$ |
| SC - 1 | $NH_4OH$: $H_2O_2$: $H_2O$ (1:1:5, 70$^oC$) | Removing particles |
| SC - 2 | HCl: $H_2O_2$: $H_2O$ (1:1:5, 70$^oC$ ) | Removing metallic ions |
| Piranha | $H_2SO_4$: $H_2O_2$ (3:1, 90$^oC$) | Removing organics and metallic ions |

**Table 1.2.** List of commonly used pre-treatments used in the IC industry.[7]

*DHF*: The first surface pre-treatment considered is etching the silicon surface using dilute HF (DHF). HF etching of silicon samples is required to get rid of the native oxide that is present on all substrates. The etching of $SiO_2$ to form hydrogen terminated silicon surfaces has been widely investigated. [8– 10] The chemical composition of HF etched surface was initially thought to be F – terminated as the Si – F bond strength (6 eV) was far greater than that of Si – H (3.5 eV).

Vibrational spectroscopic techniques clearly showed silicon-hydrogen vibrations relating to a H – terminated surface.[8, 9] The proposed mechanism for the etching reaction is given by[10, 11]

$$SiO_2 + 6HF \rightarrow 2H^+ + SiF_6^{2-}(aq) + 2H_2O \qquad (1.1)$$

or

$$SiO_2 + 4HF \rightarrow SiF_4(g) + 2H_2O \qquad (1.2)$$

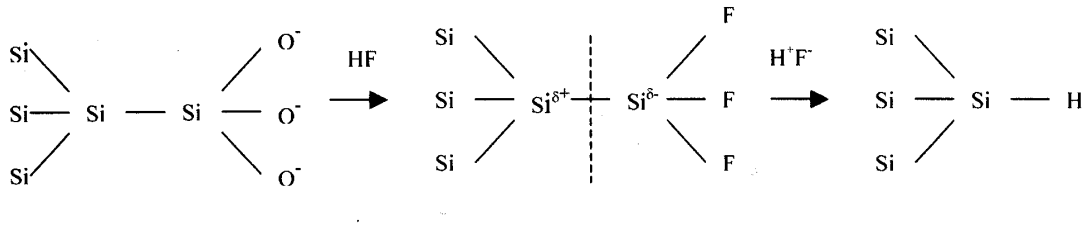


**Fig. 1.5.** HF etching of oxide covered silicon with HF.

According to Fig. 1.5, the first step is the removal of oxide leading to the formation of a F- terminated surface. The polar nature of the Si – F bond is the driving force for the polarization of the Si – Si bonds present in the second layer of the substrate (back bonds). This polarization facilitates the efficient removal of the surface silicon

bonded to F in the form of $SiF_4$ and thereby rendering a hydrogen terminated silicon surface.

*SC – 1 Clean*: SC – 1 stands for standard clean 1 solution and is another common surface cleaning technique employed in the semiconductor industry. As mentioned in Table 1.1 it is mainly used to remove particles from the silicon surface and in doing so, it leaves behind a surface covered with a chemical oxide. The role of $H_2O_2$ is to oxidize the surface while $NH_4OH$ etches the oxide. It is this cyclic process of oxidation and etching that effectively removes particles and leaves behind a clean chemical oxide.[7]

*SC – 2 Clean*: The standard clean 2 pre-treatment is used for removing metallic contamination on the silicon surface. The presence of a strong oxidant such as $H_2O_2$ ensures that the metal is oxidized into its ionic form. HCl helps in the formation of soluble complexes that can rinse off the wafer surface by a simple UPW rinse.

*Piranha:* It is commonly used to strip off photo resists and other strongly adsorbed organics from the silicon surface. $H_2O_2$ helps in removing organics while the sulphate ions remove metals by the formation of soluble complexes.

### 1.4. Metal deposition on Silicon surfaces

The deposition of metals on the silicon surface has been the basis for the functioning of the silicon-based sensor as will be seen in chapter 2. Chapter 4 also deals with sections where the effect of metal deposition on hydrogen terminated silicon surface is studied using vibrational spectroscopy. Metal deposition on H – terminated silicon surfaces has been studied in great detail by a number of researchers.[13 - 17] Only noble metals which have a more positive reduction potential with respect to hydrogen will be

plated onto hydrogen terminated silicon surfaces. Metals such as $Cu^{2+}$, $Pt^{2+}$, $Ag^{+}$, $Au^{3+}$etc. fall under this category. The deposition is essentially an electrochemical phenomenon involving the reduction of metal ions, leading to their deposition on the silicon surface and the simultaneous oxidation of the silicon resulting in its dissolution.[15]

$$M^{z+} + ze^{-} \rightarrow M^{0} \quad (1.3)$$

$$Si + 6HF + 4h^{+} \rightarrow SiF^{2-}_{6} + 6H^{+} \quad (1.4)$$

A clearer picture of the deposition process can be obtained by considering the band diagram of the silicon semiconductor along with the redox potential levels of the different metal ions known to deposit onto the silicon substrate.

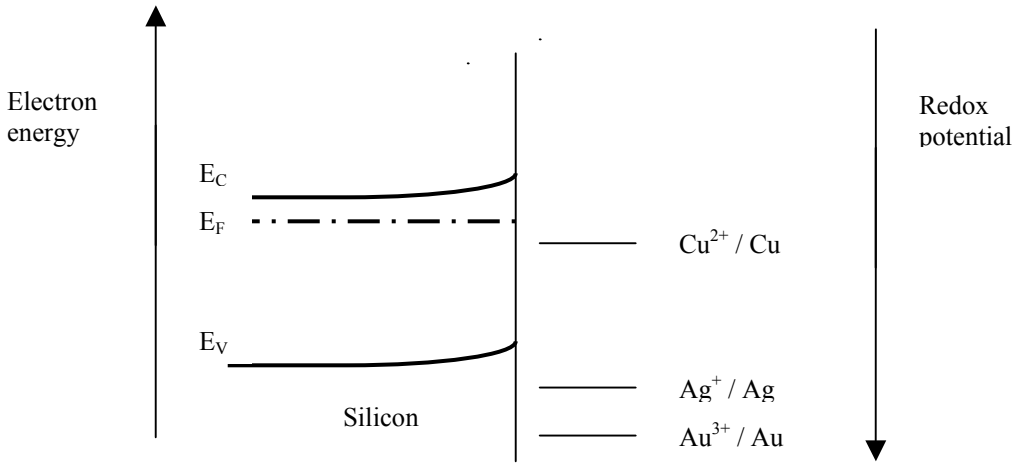


**Fig. 1.6.** Energy band diagram depicting deposition of metal ions onto *n* type Si.

In Fig. 1.6 $E_V$, $E_F$ and $E_C$ represent the position of the valence band, Fermi level and conduction band of silicon respectively. Let us consider the deposition of $Cu^{2+}$ and $Ag^{+}$ as the deposition of these two metals has been studied in this dissertation. In the case of copper, the deposition is sluggish for the following reasons:

1. The driving force for the reduction reaction of $Cu^{2+}$ is much smaller than that of $Ag^{+}$ as the reduction potential for cupric ion is 0.34V as compared to 0.8V for $Ag^{+}$.
2. The $Cu^{2+}$ / Cu redox level exists in the band gap of silicon and thus the transfer of electrons is less efficient.

On the other hand the deposition of $Ag^{+}$ is not only thermodynamically favorable but also the position of the $Ag^{+}$ / Ag redox level is in line with the valence band of silicon, which is electron rich. Thus the capture of valence band electrons by $Ag^{+}$ occurs readily. This process is commonly referred to as hole injection.

Chyan *et al.* studied the deposition of copper on hydrogen terminated silicon surfaces and found that during the initial stages of deposition the surface is covered by several nanometer-sized deposits (< 15nm diameter).[18] In other words, nucleation is the first step in the deposition process and it occurs on certain active sites. After a fixed interval of time the number of nuclei plateau out and the existing nuclei start to grow in size. This growth in the nuclei indicates that the metal ions tend to deposit on the pre-existing metal atoms. They concluded that the deposition results in the removal of several layers of silicon along with pit formation due to localized etching by HF.

### 1.5. Background and theory of FTIR – ATR spectroscopy

FTIR – ATR spectroscopy has been extensively used in the studies I have undertaken. Thus it is worthwhile to explain the theory and application of this technique. The origins of ATR spectroscopy dates back to the early 1700's when Newton observed

the phenomenon of evanescent field which is the basis of internal reflection spectroscopy.[19] Extensive research in this field was carried out after the 1970's with the

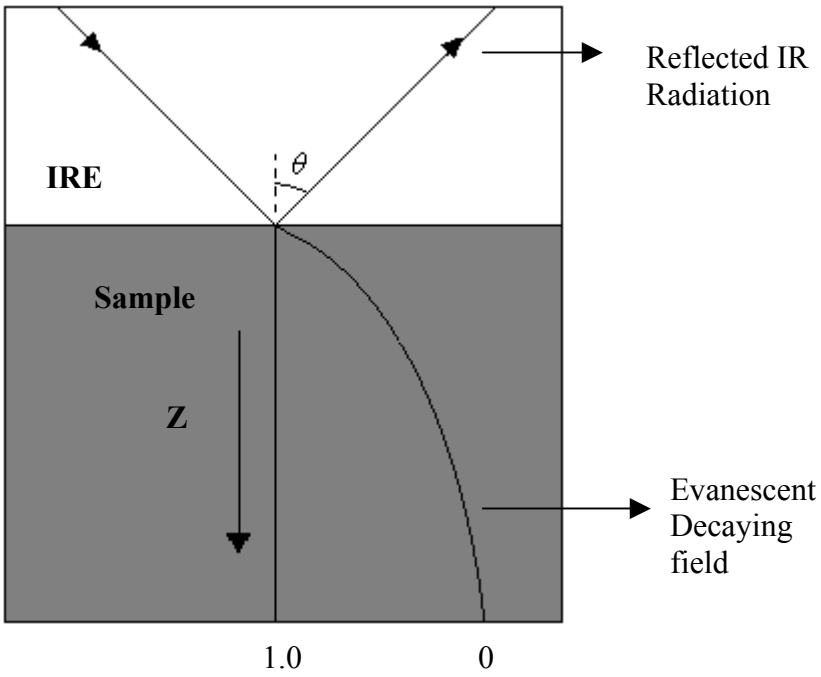


**Fig. 1.7.** Schematic of a simple IRS experiment.

advent of improved instrumentation, like availability of FTIR's and computers. This technique has proven to be an asset to the modern researcher due to the ease of the analysis and the amount of information that can be derived by it. Fig. 1.7 depicts the basic principle of internal reflection spectroscopy (IRS). The IR radiation propagates through the IRE (Internal reflection element) generating an evanescent field, which penetrates the rarer medium and decays exponentially with distance Z. For internal reflection to occur the two mediums must be in contact with each other and the medium through which the incident energy propagates must have a larger refractive index than its

counterpart. Medium 1 and medium 2 stand for the optically dense (IRE element) and rare medium (sample) respectively. Radiation propagating in medium 1 with refractive index $n_1$, undergoes total internal reflection at the interface with the optically rarer medium with refractive index $n_2$, when the angle of incidence $\theta$ exceeds the critical angle $\theta_c$. The critical angle is defined by the equation[20]

$$\theta_c = \sin^{-1} n_{21} \qquad (1.5)$$

where $n_{21} = n_2/n_1$. Under these conditions the evanescent wave is considered to have the following properties

a) It is non-transverse and has components in all spatial directions
b) The electrical component of the evanescent field extends into medium 2 and decays exponentially with distance in the z direction.
c) There is a displacement of incident and reflected waves due to energy flow parallel to the surface.

If $E_o$ is considered to be the amplitude of incident energy, then E, the amplitude of the evanescent field can be expressed as[20]

$$E = E_o \exp - [\frac{2\pi}{\lambda_1} (\sin^2\theta - n_{21})^{1/2} Z] \qquad (1.6)$$

$\lambda_1 = \lambda/n_1$ is the wavelength of radiation in medium 1, $\lambda$ is the wavelength in air and Z is the distance from the surface. This equation was further modified by Harrick[19] who rightly took into account the absorption of energy in the rarer medium, which is indeed essential for a measurement to be made.

$$E = E_o \exp [-\gamma Z] \qquad (1.7)$$

$$\gamma = \frac{2\pi(\sin^2\theta - n_{21}^{\,2})^{\frac{1}{2}}}{\lambda_1} \qquad (1.8)$$

The penetration depth of the evanescent field ($d_p$) was defined as $Z = d_p = 1/\gamma$ which would occur when E decays to $E_o$ exp [-1].

$$d_p = \frac{\lambda_1}{2\pi(\sin^2\theta - n^2{}_{21})^{\frac{1}{2}}} \qquad (1.9)$$

From the equation pertaining to $d_p$, one could draw the following conclusions:

a) As $n_{21} \rightarrow 1$, $d_p$ increases. This implies that as index matching increases the decay constant decreases resulting in increase of $d_p$.

b) Increase in $\lambda_1$ results in an increase in $d_p$.

c) In the case of very thin films the evanescent wave can be considered to be un-attenuated. Thus neither the decay constant $\gamma$ nor the wavelength has any effect on $d_p$.

*IRS Elements:* Some of the common IRS elements that are used are KRS- 5, AgCl, AgBr, Ge and Si. The choice of the IRS element depends mainly on the on the kind of sample being analyzed. The refractive index of the element obviously has to be higher than that of the sample for internal reflection to occur. KRS – 5 is a common name for Thallium Bromo Iodide and is widely used as a ATR element for analyzing organic compounds, especially polymers. In my research Si was used as the IRE element. The advantage of Si lies in the fact that cleaning of the ATR element with appropriate chemistries was possible thereby ensuring multiple use of the same element.

| IRE | Refractive Index |
|---|---|
| KRS - 5 | 2.37 |
| AgCl | 1.98 |
| AgBr | 2.16 |
| Si | 3.42 |
| Ge | 4 |

**Table 1.3.** List of commonly used ATR elements.

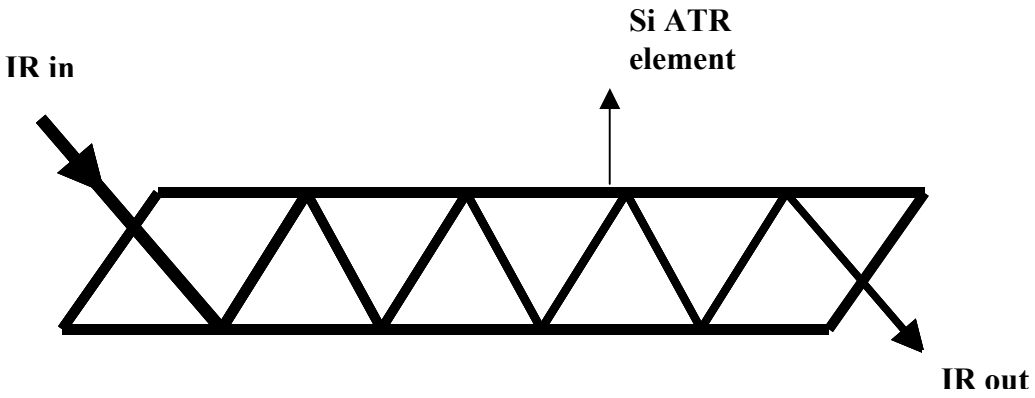


**Fig. 1.8.** Schematic representation of MIRIS with a Si ATR element.

Figure 1.8 shows a schematic depicting the multiple internal reflection spectroscopy (MIRIS) technique using Si as an IRS element. IR beam is incident normal to the surface of the ATR element, which has a bevel angle of $45^{o}$. Multiple internal reflections occur due to the difference in the refractive indices of the bulk substrate and the surface within the length of the element. Each internal reflection sets up a standing wave pattern (evanescent wave) due to the interference of the incoming and outgoing waves, which is confined to sub-micron space above the silicon surface. The electrical component of this evanescent wave can detect up to a sub-monolayer of adsorbed species on the silicon

surface by nature of its interference with the interface. The number of internal reflections can be obtained using the following equation

$$N = l / t \,.\, \cot\theta \qquad (1.18)$$

Where N is the number of reflections, *l* and *t* are the length and thickness of the ATR element respectively. In my studies I had used a Si ATR element which was 6cm long and ~0.6mm thick. The bevels of the Si ATR element were shaped to have an angle of $45^{o}$, thus the number of internal reflections that occurred were ~100. The advantage of MIRIS is that it makes use of the number of internal reflections to amplify weak signals as a result of which the sensitivity is increased.

## 1.6. Chapter References


1. R. C. Jaeger, Introduction to Microelectronic Fabrication, Addison-Wesley Publishing Company Inc., U.S.A., 1988.
2. P. V. Zant, *Microchip Fabrication: A Practical Guide to Semiconductor Processing*, McGraw – Hill (1997).
3. A. Lester, *Semiconductor* M. *International,* **25**, 40 (2002).
4. O. M. R. Chyan, J. J. Chen, H. Y. Chien, J. J. Wu, M. Liu, J. A. Sees and L. H. Hall, *J. Electrochem. Soc.,* **143**, 235 (1996).
5. F. A. Cotton and C. Murillo, *Advanced Inorganic Chemistry*, John Wiley & Sons (1999).
6. H. N. Waltenburg and J. T. Yates, *Chem. Rev*., **95**, 1589 (1995).

7. W. Kern*, Handbook of Semiconductor Wafer Cleaning Technology*, Noyes Publications, Park Ridge, NJ (1993).

8. V. A. Burrows, Y. J. Chabal, G. S. Higashi, K. Raghavachari and S. B. Christman, *Appl. Phys. Lett.,* **53**, 998 (1988).

9. Y. J. Chabal, G. S. Higashi, K. Raghavachari and V. A. Burrows, *J. Vac. Sci. Technol.*, **A7**, 2104 (1989).

10. G. S. Higashi, Y. J. Chabal, G. W. Trucks and K. Raghavachari, *Appl. Phys. Lett.*, **56**, 656 (1990).

11. K. Raghavachari, G. S. Higashi, Y. J. Chabal and G. W. Trucks, *Mat. Res. Soc. Symp. Proc.*, **315**, 437 (1993).

12. S. Verhaverbeke, H. Bendar, M. Meuris, P. W. Mertens, H. F. Schmidt and M. M. Heyns, *Mat. Res. Soc. Symp. Proc.*, **315**, 457 (1993).

13. I. Teerlinck, P. W. Mertens, H. F. Schimdt, M. Meurius and M. M. Heyns, *J. Electrochem. Soc.,* **143**, 3323 (1996).

14. L. Mouche, F. Tardif and J. Derrien, *J. Electrochem. Soc.,* **142**, 2395 (1995).

15. P. Gorostiza, R. Diaz, J. Servat and F. Sanz, *J. Electrochem. Soc.,* **144**, 909 (1997).

16. G. J. Norga, M. Platero, K. A. Black, A. J. Reddy, J. Michel and L. C. Kimerling, *J. Electrochem. Soc.,* **144**, 3323 (1997).

17. T. Homma, C. P. Wade and C. E. D. Chidsey, *J. Phys. Chem. B*, **102**, 7919 (1999).

18. O. M. R. Chyan, J. J. Chen and H. Y. Chien, J. A. Sees and L. Hall, *J. Electrochem. Soc.,* **143**, 92 (1996).

19. N. J. Harrick, Internal Reflection Spectroscopy, Interscience Publishers: N.Y. (1967).

20. F. M. Mirabella, N. J. Harrick, Internal Refletion Spectroscopy: Review and Supplement, Harrick Scientific Corporation, N. Y. (1985).

CHAPTER 2

# MONITORING METAL ION CONTAMINATION ONSET IN HYDROFLUORIC ACID USING SILICON-DIAMOND AND DUAL SILICON SENSING ELECTRODE ASSEMBLY

## 2.1 Introduction

The purity of the silicon wafer surface is an essential prerequisite for the successful fabrication of ultra large-scale integrated silicon circuits. Many wafer-cleaning methodologies were developed to remove trace impurities, such as ions, metals and particles from silicon surface prior to high temperature processing (thermal oxidation, epitaxial growth, and diffusion). The chemistry based on sequential hydrogen peroxide chemical oxidation, chloride complexation and hydrofluoric acid (HF) etching is generally the most utilized cleaning approach for silicon wafers before metallization. To ensure optimal fabrication yield, various chemical cleaning baths are carefully monitored by periodic sampling off the production line for impurities.

Recently a new class of silicon-based sensors that can sensitively detect parts-per-billion (ppb) to parts-per-trillion (ppt) levels of ionic impurities in hydrofluoric acid, alkaline hydrogen peroxide solution and ultra pure water has been reported.[1-3] In HF solutions, trace levels of metal ion impurities like $Ag^{+}$, $Cu^{2+}$, $Au^{3+}$, $Pt^{2+}$ and $Pd^{2+}$ can be readily reduced and deposited as zero-valence metal nanoparticles on an oxide-free silicon surface.[4] The nano-scale metal

deposition shifts the silicon potential more positively to afford below ppb detection sensitivity. The ultra-sensitive detection capability makes the silicon-based sensor useful in online monitoring of the metal contamination onset and assuring the chemical purity at the point of use. More importantly, the silicon-based sensor has the important advantage of being made completely compatible and can be incorporated into the actual integrated circuits (IC) device fabrication processes designed for silicon materials. However, a non-contaminating stable reference electrode is needed to accompany the potentiometric silicon-based sensor in the practical online monitoring application.

Conventional calomel and Ag/AgCl reference electrodes with free flow capillary or leaky ceramic junctions are suitable for the general potentiometric analyses, but will cause detrimental contamination in the ultra pure chemical baths used in IC fabrication. According to reported literature, to avoid the leakage problem, the internal liquid electrolyte is generally protected by a polymeric membrane layer or is replaced by embedding the electrolyte in a polymer membrane matrix.[5-7] In another interesting approach, the reference electrode is made from two separate anion and cation conductive membranes coated on Ag/AgCl electrodes connected in parallel.[8] However, the chemical stability of Ag/AgCl based solid-state reference electrodes can be compromised in corrosive environments, such as HF acid baths. In this chapter two different approaches that were used to prepare the non-contaminating reference electrodes for the silicon sensor assembly is being reported. In the first case, a conductive diamond electrode was used as a non-contaminating quasi reference electrode. Cyclic voltammetric studies with a standard redox couple indicated that the conductive diamond is suitable for functioning

as a reference electrode. In the other approach, an additional silicon electrode protected by an anion permeable membrane was used as the reference electrode. The latter approach allows both the sensing and reference electrodes to be derived solely from the regular silicon wafer and has a greater potential to be applied in the on-line monitoring application for IC chemical processing.

## 2.2. Experimental

Diamond electrode preparation: Polycrystalline diamond films (ATM Inc.) were grown on Si (100) (p-type, 0.01 Ω.cm) substrates in a hot-tungsten filament assisted chemical vapor deposition system. The wafers were cut into (1cm x 1cm) chips, and then treated with 10% $HNO_3$ for 10 minutes and etched in 4.9% HF for 5 minutes followed by an ultrapure water rinsing. The electrical contact was made to the backside of the diamond chip using Ga/In eutectic (99.99%, AESAR). The diamond chip was then encapsulated in a custom-made perfluoroalkoxy polymer (PFA) electrode body, which allows solution contact only to the front side of the diamond chip.[6]

Potential controlled experiments were carried out using a freestanding diamond film. The freestanding films were obtained by peeling off the film from the silicon substrate. The remaining silicon residue was cleaned using a selective etching solution ($HNO_3/CH_3COOH/HF$, 67:25:8 w/w %). An alligator clip was used to hold the thin film diamond during the course of the experiment.

Silicon electrode preparation: Two different configurations were used for the silicon electrode assembly. In the first case, the silicon chip derived from single crystal n-Si

arsenic doped wafers was encapsulated in a PFA electrode body similar to the one used for the diamond electrode for the OCP measurements.[1] In the second method the silicon sensing electrodes were prepared from single crystal n-Si arsenic doped wafers. They were first cut into 3 cm x 1 cm dimensions and were then subjected to standard silicon wafer cleanings (HF, $NH_4OH/H_2O_2$, $HCl/H_2O_2$).[9] The silicon chips were held by specially designed clamps, which were covered with gold foil to ensure proper ohmic contact. The $Ag^+$/HF solutions were prepared by dissolving $Ag_2SO_4$ (99.999%, Puratronic, Aesar) in electronic grade HF solution. All PFA labware were cleaned by boiling them in 10% $HNO_3$ thrice followed by ultrapure water ($R > 18.2\ M\Omega$) rinse prior to running the experiments.

Pre-treatment of Anion Membranes: Anion selective membranes provided by Millipore Corporation were used for the experiments. These membranes were designed to be selectively permeable to $F^-$ ions. The membranes were conditioned by cutting them to 2 cm x 2 cm dimensions and by soaking in hot ultrapure water ($80^oC$) for 15 minutes. For the purpose of cleaning they were soaked in 10% HCl for 1 hour followed by rinsing in ultrapure water. This cleaning process was carried out three times after which the membranes were soaked in a 0.01% HF solution for a minimum of 24 hours before being used in experiments. The pre-treated membranes were sealed in a specially designed PFA tube prior to the start of each experiment.

Instrumentation: The open-circuit potential of the sensing electrodes was measured with respect to a double junction standard Ag/AgCl reference electrode (Orion, Model

900200) using a computer interfaced, high input impedance potentiometer (Accumet 50, Fisher Scientific) under normal room light conditions. The outer epoxy body of the reference electrode was thoroughly rinsed with ultrapure water and the outer junction solution (10% $KNO_3$) replenished before each experiment. Potential controlled experiments were performed using an EG&G 273 potentiostat in a standard three-electrode cell with a platinum counter electrode and Ag/AgCl reference electrode. ICP/MS (Fisons, Model PQS) and graphite furnace atomic absorption spectroscopy (GFAA, Varian SpectraAA 330/400) were used to analyze the purity of the sample solutions. Atomic force microscope (AFM, Nanoscope III, Digital instruments) operated in the tapping mode was used to image the silicon sensor surface. Scanning electron microscopy (SEM) was performed with a JEOL JSM-T300 electron microscope.

## 2.3. Results and Discussion

Fig. 2.1 depicts the time dependent potentiometric response of a silicon-sensing electrode with respect to a double junction Ag/AgCl reference electrode in 0.01% HF solution. It has been previously reported that the open-circuit potential of a hydrogen terminated silicon electrode is rather stable in a pure HF solution.[4] However, the silicon potential will drastically increase in the presence of trace metal impurities in HF. As observed in Fig. 2.1, the potential remains stable for only ca. 15 hours, after which there was an abrupt positive shift of the silicon potential indicating that the silicon electrode was contaminated. AFM analysis of the silicon sensor electrode confirmed that nanometer-sized deposits were present on the silicon surface. [10]

For a reference electrode to function optimally there has to be a steady flow (3-30 µl/hr) of the filling electrolyte through liquid junctions into the test solution. [11]

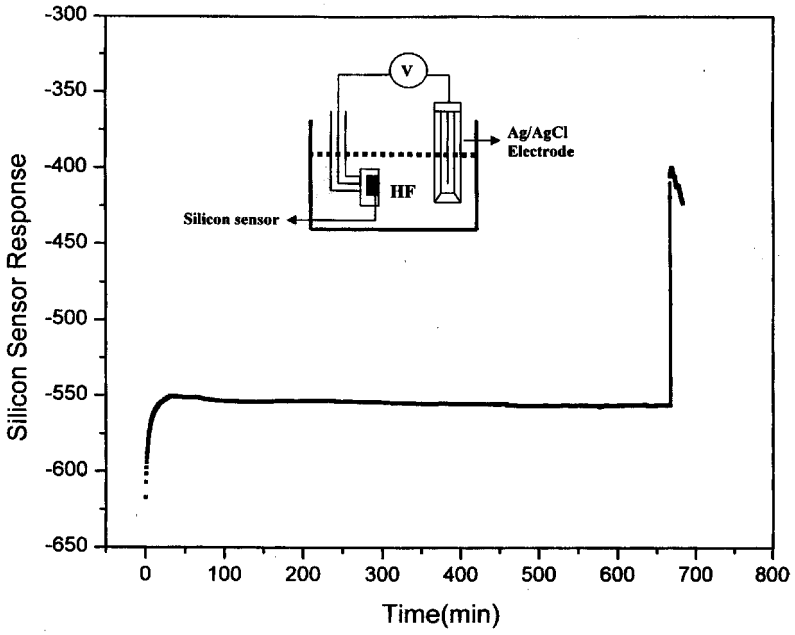


**Fig. 2.1.** Time dependent potential response of a silicon-sensing electrode in 0.01% HF with respect to Ag/AgCl reference electrode.

The observed abrupt change in the open-circuit potential of the silicon-sensing electrode is due to the leakage of silver containing electrolyte into HF solution from the inner body of the Ag/AgCl reference electrode. To delay the onset of reference electrode contamination, a double junction configuration was employed to initially contain the electrolyte leakage in the outer junction $KNO_3$ solution. However, a non-contaminating reference electrode is clearly needed for the silicon-based sensor to be effectively used in a continuing operation mode like monitoring HF etching baths for IC processing.

### 2.3.1. Diamond as a Quasi-reference electrode

The essential characteristics of a suitable reference electrode for the silicon-based sensor are that; they should be non-contaminating, stable and chemically inert especially in the highly corrosive chemical environments used in semiconductor processing. Most of the junction-free reference electrodes reported in the literature cannot meet all of these requirements.[12] The growth of polycrystalline diamond thin films by chemical vapor deposition has been well established. The synthetic diamond thin films possess several technologically important properties: hardness, corrosion resistance, high thermal conductivity, chemical inertness, dimensional stability and conductive nature due to doping.[13,14] The thin film diamond was considered as a quasi reference electrode due to the above mentioned desirable properties. To verify the chemical inertness of diamond electrode in HF solution, a diamond sample was placed in HF solution for 24 hours and the HF solution was analyzed with ICP/MS and GFAA. The analysis indicated that no metallic contaminants were present above the detection limits (ca. 1 ppt) of the instruments. To further verify the chemical inertness of diamond, a freestanding diamond film was placed in a 1 ppm $Ag^+$/HF solution for 1 hour. No Ag deposits were observed on the diamond surface under SEM and EDX analysis. Separate measurements were also carried out to evaluate the potentiometric response of diamond electrode in HF solution in the presence of 1 ppb to 10 ppm $Ag^+$.

Fig 2.2 depicts the open circuit potential response of the diamond electrode in 0.01% HF with respect to Ag/AgCl reference electrode. There seems to be a long period (~50 min) of equilibration between the diamond electrode surface and the HF solution. Once a stable base line was established, known amounts of $Ag^+$ was added to the system.

As can be seen in Fig. 2.2 no change in the potential is observed for additions ranging from 10 ppb – 1 ppm indicating the stability and chemical inertness of the diamond electrode. There is a shift in potential only after the addition of 10 ppm of $Ag^+$. This is caused as the solution potential dominates at such high concentrations. As the use of a silicon-based sensor was being considered to detect metallic contaminants in semiconductor process chemicals, it is safe to assume that one would not encounter such high levels of contamination. Thus the silicon-based sensor in conjunction with the diamond reference electrode would be a good candidate for detecting ppb to ppt levels of metallic contaminants.

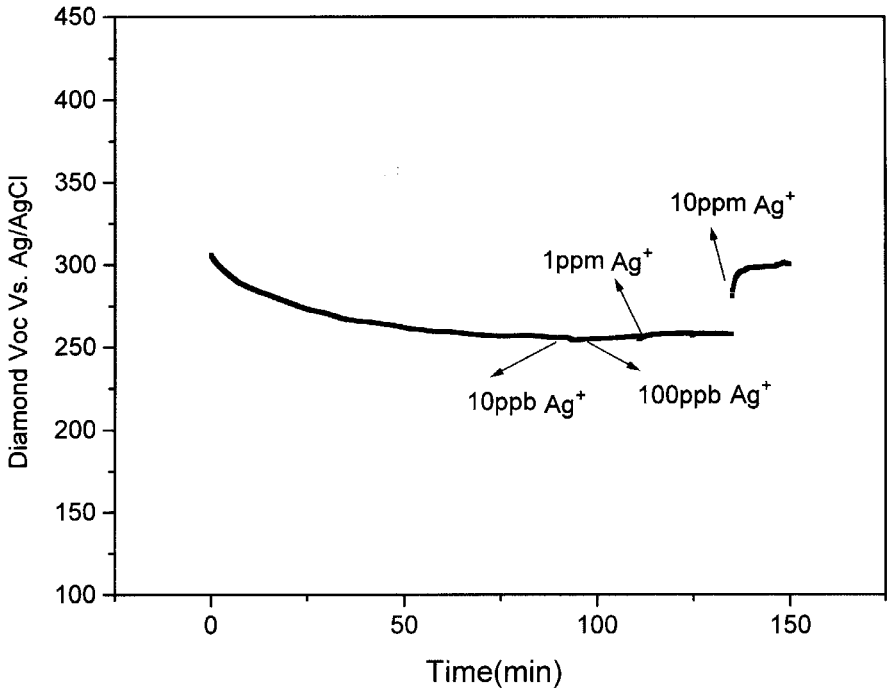


**Fig. 2.2.** Open circuit potential response of thin film diamond electrode in 0.01% HF followed by additions of varying amounts of $Ag^+$.

To evaluate the effectiveness of the diamond reference electrode potential controlled experiments were carried out using Ferro/Ferricyanide redox couple. Fig. 2.3 shows a set of cyclic voltammograms of $Fe(CN)_6^{3-/4-}$ redox couple for different scan rates using diamond as a reference electrode and glassy carbon as a working electrode. The cyclic voltammograms indicate that the formal reduction potential of $Fe(CN)_6^{3-/4-}$ redox couple is stable with the change in the scan rate and the plot of peak current versus $\nu^{1/2}$ (scan rate) gives a linear response as expected for a fast reversible electron transfer system.

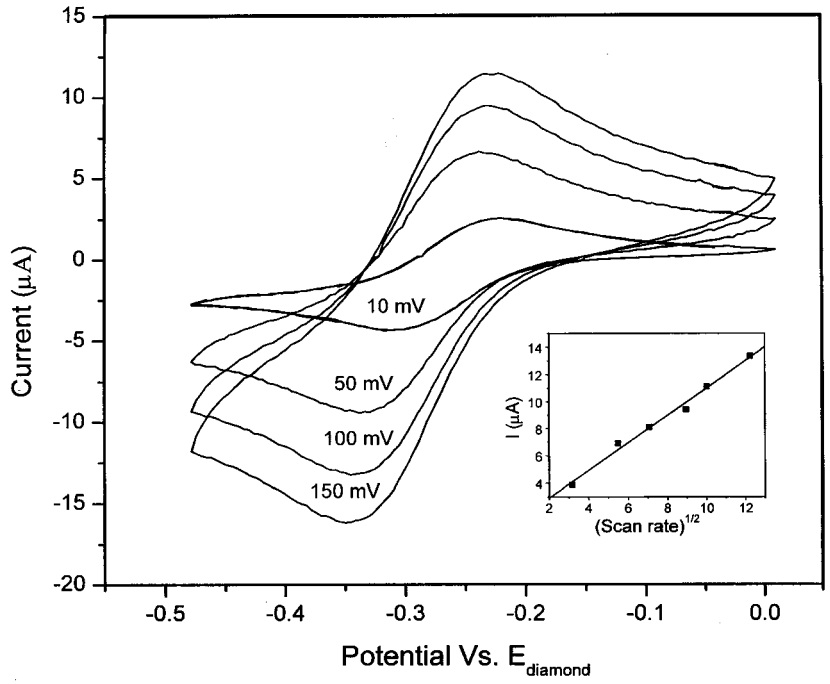


**Fig. 2.3.** Cyclic voltammograms of glassy carbon electrode using thin film diamond as a quasi-reference electrode in 0.1 mM $K_3Fe(CN)_6$ – 0.1 M NaCl – 0.01% HF for different scan rates. Inset corresponds to the plot of peak current vs. $(\nu)^{1/2}$.

This further validates the point that diamond does possess favorable qualities to be used as a quasi-reference electrode for electrochemical measurements.

Fig. 2.4 shows the time dependent potential response of a silicon-sensing electrode with respect to a diamond quasi-reference electrode.

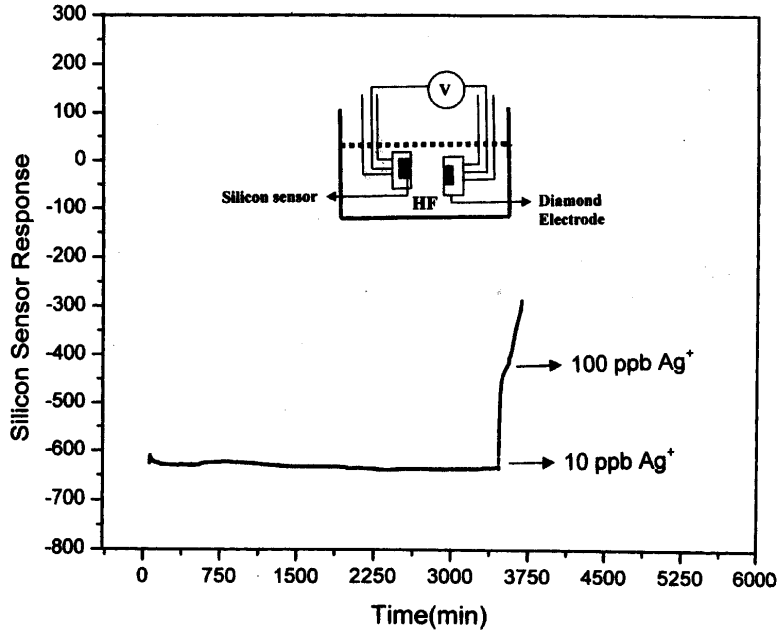


**Fig. 2.4.** Silicon sensor response using conductive diamond as a quasi reference electrode in 0.01% HF followed by the addition of 10 ppb and 100 ppb of $Ag^{+}$.

As can be seen, a relatively stable silicon sensor potential background (± 8 mV) was maintained for at least 57 hours when the diamond quasi-reference electrode was used. At the end of 57 hours, 10 ppb of $Ag^{+}$ was intentionally added to the HF solution to simulate an actual onset of metal ion contamination. The observed abrupt potential jump indicated that the silicon-based sensor retains its sensing capacity to detect trace amounts of metallic contaminants even after 57 hours of continual operation.

Although diamond has the above-mentioned favorable properties as reference electrode, it has its drawbacks. In addition to the diamond film being fairly expensive, the potential of the diamond quasi-reference electrode can be changed by the pH of its

contacting solution. The diamond films used in this study was hydrogen-terminated as prepared.[15] We postulate that the potential of the diamond electrode is held by some equilibrium reaction between the hydrogen-terminated diamond surface and the protons in the solution. A change in the proton concentration will cause a shift in the diamond potential. For a chemical system with relatively stringent control on pH, like IC processing chemical baths, diamond quasi-reference electrode should perform well with the silicon-based sensor. Another useful observation is that the diamond quasi-reference potential drift due to the solution pH change was a slower process in comparison to the abrupt potential increase caused by metal ion contamination on silicon sensor electrode when using Ag/AgCl as the reference electrode. In principle, with proper analysis of the potential dynamic responses, the more detrimental metal ion contamination onset can be identified.

### 2.3.2 Quasi-reference electrode based on Silicon/Anion membrane configuration

The important advantage of the silicon-based chemical sensor is that it can be made completely compatible and can be incorporated into the actual IC device fabrication processes designed for silicon material. Although diamond quasi-reference electrode is a good candidate for solving the contamination problems originating from the leaky conventional reference electrode, it would be ideal if the reference electrode could be derived from the silicon wafer in order to maximize the compatibility. Liu *et al.* previously reported a dual ion-selective electrode-flow injection system that did not contain a conventional reference electrode and no liquid junction was present.[16] The system was successfully

applied to simultaneously determine the presence of fluoride/nitrate, sodium/potassium and nitrate/potassium in the natural waters. The operational requirement is that no cross-contamination should occur between two ion-selective electrodes that are operated in parallel. Our strategy is to use a dual silicon electrode system and protect one of the silicon electrodes by an anion permeable membrane to function as a quasi-reference electrode. The anion permeable membrane is designed to block the flow of metal cations and prevent the contamination of the silicon reference electrode thereby maintaining a constant potential.

To verify the effectiveness of the membrane, the potential of a silicon-based sensor was monitored with respect to a Ag/AgCl reference electrode which was isolated from silicon-based sensor with an anion permeable membrane. As previously demonstrated in Fig. 2.1, the leakage of Ag/AgCl reference electrode will contaminate silicon sensor within 15 hours. With the protection of the anion membrane, the silicon potential can remain stable for several days without contamination.

For instance, Fig. 2.5 shows the silicon sensor can sensitively detect a simulated contamination onset of 500 ppt $Ag^+$ via a rapid increase of silicon potential deviation from a stable silicon potential background after 67 hours of non-stop monitoring. The fact that a stable potential is maintained for such a long duration indicates that the anion membrane is effective in preventing the effusing metallic species leaking through the reference electrode from reaching the sensing electrode surface. Another important point is that the anion permeable membrane

was shown to be chemically stable in the corrosive HF acid environment and did not curtail the highly desirable detection sensitivity of the silicon-based sensor.

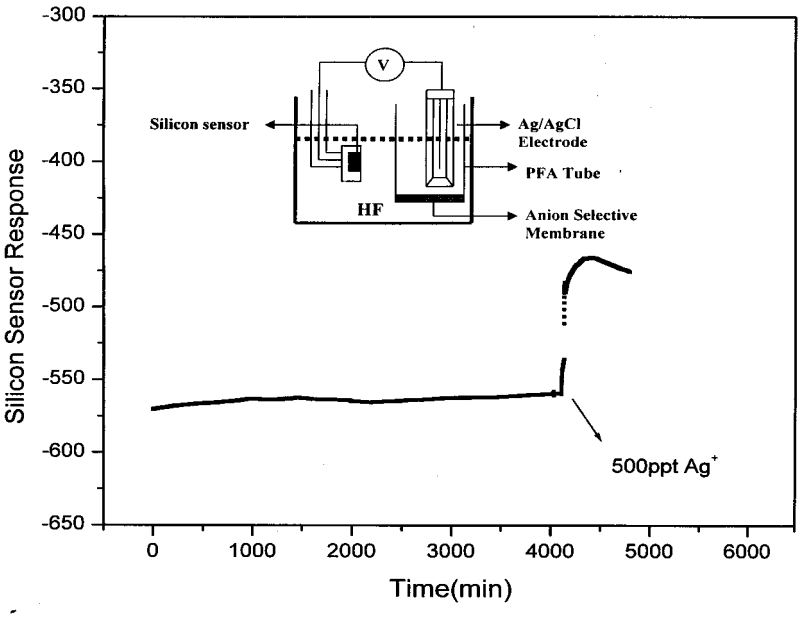


**Fig. 2.5.** Potentiometric response of silicon-based sensing electrode protected by an anion permeable membrane in 0.49% HF followed by addition of 500 ppt of $Ag^{+}$.

Once the effectiveness of the anion specific membrane was established, the dual silicon electrodes and anion permeable membrane configuration was tested. As shown in Fig. 2.6, the silicon electrode behaving as the reference electrode was sealed within the PFA tube with the anion specific membrane. Fig. 2.6 shows that the silicon sensor response for the new sensor configuration was stable for over 30 hours and on the addition of just 100 ppt of $Ag^{+}$ there was a shift in potential of over 100mV in the positive direction. On addition of higher concentrations of $Ag^{+}$, a more positive silicon potential shift was observed. In addition to $Ag^{+}$, other metal ions including $Cu^{2+}$, $Au^{3+}$,

$Pt^{2+}$ and $Pd^{2+}$ can also be sensitively detected by the new dual silicon electrode/membrane configuration.

The results indicate that the new silicon-based sensor assembly can effectively detect trace metal ion impurities at the ppt level, which is the sensitivity requirement for the state-of-art IC processing control.

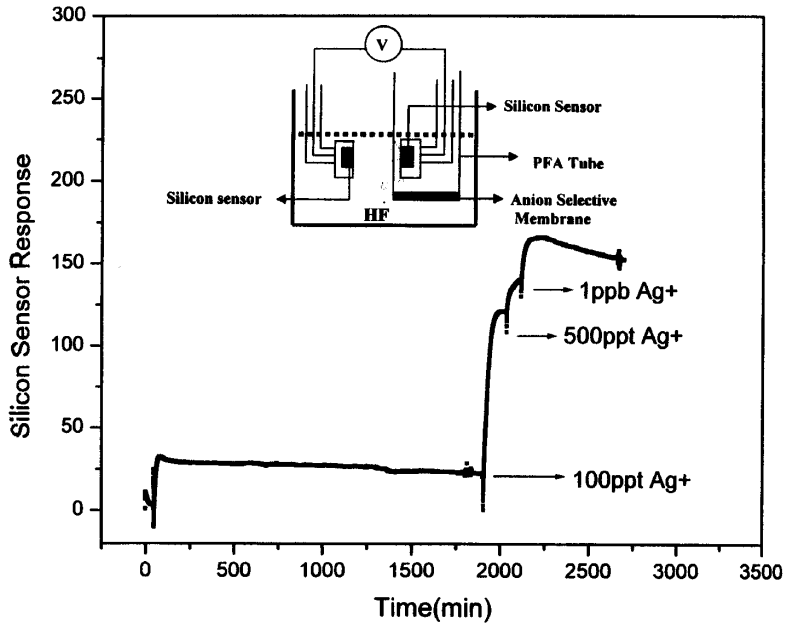


**Fig. 2.6.** Potentiometric response of a dual silicon electrode system in 0.01% HF followed by addition of 100 ppt - 1 ppb $Ag^{+}$. The reference electrode is a silicon electrode protected by an anion permeable membrane.

Another important observation is that the sensor response from the new sensor assembly is practically independent of the solution acidity. Since the new sensor assembly derives both the sensing and the reference electrodes from the silicon wafer, any difference in potential is nullified. These experimental data have shown that there

were differences of only 6 mV in the silicon potential background in 0.01% and 0.49% HF solutions.

In summary, two types of non-contaminating reference electrode systems were developed in this work to assist the silicon-based potentiometric sensor for detecting ppt levels of trace metallic contaminants in HF under simulated long term monitoring conditions. Both diamond quasi-reference electrode and the dual silicon electrode/membrane configurations possess the essential requirements of a suitable reference system. They are non-contaminating, stable and chemically inert especially in the highly corrosive chemical environments used for semiconductor processing. These data have demonstrated that the dual silicon electrode design have two additional advantages, i.e. excellent compatibility and independence from solution acidity, and can thus be used in the online detection of metallic contaminants in HF baths for microelectronics applications.

## 2.4. Chapter References


1. *VLSI Technology*; S.M. Sze ed.; McGraw Hill: New York, 1988.
2. *Handbook of Semiconductor Wafer Cleaning Technology*, W. Kern ed.; Noyes Publications, Park Ridge, New Jersey, 1993.
3. (a) W. Kern, *RCA Review*, Part I: **31**, 207(1970). ; Part II: **31**, 234(1970). ; Part III: **32**, 64(171). (b) D. Riley, and R. Carbonell, *Proc. of The Institute of Enviromental Sciences Ann. Tech, Mtg.,* pp 224-228, New Orleans, LA (1990). (c) W. Kern, *J. Electrochem. Soc.*, **137**, 1887 (1990). **(**d) H. Kikyuama, N. Miki,

K. Saka, J. Takano, I. Kawanabe, M. Miyashita and T. Ohmi, *IEEE Trans. Semicond. Manufact.,* **4**, 26 (1991).

4. O. Chyan, J.J. Chen, H.Y. Chein, J.J. Wu, M. Liu, J. Sees and L. Hall, *J. Electrochem* Soc., **143**, L235 (1996).
5. O. Chyan, J.J. Chen, L. Chen and F. Xu, *J. Electrochem* Soc., **144**, L18 (1997).
6. O. Chyan, J.J. Chen, F. Xu, J. Sees and L. Hall, *Analyst*, **125**, 175, (2000).
7. (a) T. Ohmi, T. Imaoka, I. Sugiyama and T. Kesuka, *J. Electrochem* Soc., **139**, 3317 (1992). (b) M.L. Kniffin, T.E. Beerling and C.R. Helms, *J. Electrochem* Soc., **139**, 1195 (1992). (c) L.A. Nagahara, T. Ohmori, K. Hashimoto and A. Fujishima, *J. Vac. Sci. Technol*., **A11 (4)**, 763 (1993).
8. H.J. Lee, U.S. Hong, D.K. Lee, J.H. Shin, H. Nam and G.S. Cha, *Anal. Chem*., **70**, 3377 (1998).
9. H. Suzuki, H. Shiroishi, S. Sasaki and I. Karube, *Anal. Chem*., **71**, 5069 (1999).
10. H. J. Yoon, J.H. Shin, S.D. Lee, H. Nam, G.S. Cha, T.D. Strong and R.B. Brown, *Sensors and Actuators B*, **64**, 8 (2000).
11. K. Nagy, K. Eine, K. Syverud and O. Aune, *J. Electrochem* Soc., **144**, L1 (1997).
12. O. Chyan, J.J. Chen, H.Y. Chein, J. Sees and L. Hall, *J. Electrochem* Soc., **143**, 92, (1996).
13. (a) P. Allongue, V. Costa-Klieng and H. Gerischer*, J. Electrochem. Soc.,* **140**, 1018 (1993); (b) P. Allongue, V. Costa-Klieng and H. Gerischer, *Electrochim. Acta*, **40**, 1353 (1995); (c) M. Niwano, T. Miuara and N. Miyamoto*, J. Electrochem. Soc.*, **145**, 659 (1998).

14. D.T. Sawyer and J.L. Roberts, *Experimental Electrochemistry for Chemists*, Wiley-Interscience Publication, NY (1974).

15. (a) D.T. Sawyer, A. Sobkowiak and J.L. Roberts, *Electrochemistry for Chemists*, Wiley-Interscience Publication, NY (1995). (b) A.K. Covington*, Ion–Selective Electrode Methodology*, Vol. 1, CRC Press Inc., Florida (1979). (c) D.J.G. Ives, G.J. Janz, *Reference Electrodes*, Academic Press Inc. N.Y. (1961).

16. (a) K.E. Spears and E.J.P. Dismukes, Eds.; *Synthetic Diamond: Emerging CVD Science and Technology*; John Wiley and Sons: New York, 1994. (b) L.S. Pan; D.R. Kania,, Eds., *Diamond: Electronic Properties and Applications*, Kluwer Academic Publishers, Boston, 1995. (c), J. C. Angus; C. C. Hayman,, *Science*, , **241**, 913. (1988).

17. (a) J. Xu, M.C. Granger, Q. Chen, J.W. Strojek, T.E. Lister and G.W. Swain, *Anal. Chem*., **69**, 591A (1997). (b) J. Wang, G.M. Swain, T. Tachibana, and K. Kobashi, *Electrochem. Solid State Lett.*, **3**, 286 (2000) (c) L.F. Li, D. Totir, B. Miller, G. Chottiner, A. Argoitia, J.C. Angus, and D.A. Scherson, *J. Am. Chem. Soc.,* **119**, 7875 (1997).

18. J.B. Miller, and G.R. Brandes, *J. Appl. Phys.,* **82**, 4538 (1997).

19. M.R. Liu, D.J. Liu and A.L. Sun, *Analyst*, **117**, 1335 (1992).

CHAPTER 3

# DETECTION OF NICKEL USING ATTENUATED TOTAL REFLECTION INFRARED SPECTROSCOPY

## 3.1. Introduction

Detection of metal contaminants such as Ni, Cr, As, Cd, Hg etc. in the environment continues to receive a lot of research attention due to their adverse effects on human and aquatic species.[1,2] Field surveys and testing are commonly the first steps to provide necessary information for environmental remedial undertaking. Due to the inherent complexity of sampling and handling issues, it is economical and efficient to analyze the metal contaminants right at the contaminated site. In general, selectivity, low detection limits, rapid analysis and low costs are main factors in designing new techniques for the field detection of such metals.

The impact of nickel and its compounds on aquatic species and humans has been systematically studied.[3] According to EPA regulations, the recommended water quality criteria for nickel to be considered for human consumption is below 0.6 ppm. It was found that [ $Ni^{2+}$] > 1 ppm level in the aquatic environment proved to be lethal to several aquatic species. Long-term effects of exposure to lower ppb levels of nickel in these water bodies have adverse effects on the reproductive ability of the aquatic biota. The human species too have not been left untouched by this silvery metal and its compounds. It has been found that contact with solutions of nickel salts may result in dermatitis and exposure to nickel carbonyl can lead to cancer.

The techniques employed for the detection of nickel are well established. Some of the common techniques employed include gravimetry, atomic absorption spectroscopy, mass spectrometry[4,6], and spectrophotometry.[7] Though low detection limits are possible using these techniques, high operation cost and elaborate sample preparation requirements make it unsuitable for field-testing. Some of the techniques employed for field-testing are electroanalytical techniques[8-10], chemical spot testing, colorimetric analysis, ion exchange and adsorption, co-precipitation etc..[4,5] Although some success has been reported using the above methods, complex matrices (like dissolved organics and colloidal particles) of the environmental sample can quickly foul up the sensor's response and limit its detection sensitivity.

This chapter deals with developing a novel method for the detection of $Ni^{2+}$ using silicon attenuated total reflection (ATR) infrared sensor. Quantitative ATR technique have emerged as a useful analytical tool for quick, sensitive and reliable analyses.[11-14] Thin film planar waveguides, which generate numerous internal reflections and thereby enhance sensitivity, have been effectively used as chemical sensors.[15,16] Tomellini *et al*. had used PVC(polyvinylchloride)/Chloroparaffin coatings on their ATR element to improve the detection of organic compounds,[17] while MacCraith *et al*. have used a similar kind of coating on their ATR element for the detection of pesticides. Silicon ATR crystal have been successfully utilized to detect trace organic contaminants in electronics grade hydrofluoric acid.[18] In the present work, the $Ni^{2+}$ sensing capacity was added to the silicon ATR element with a uniform coating of dimethylglyoxime (DMG) probe molecules in Nafion matrix. Nafion polymers (Fig. 3.1) are sulphonated fluorocarbons, which are chemically inert and have high permeability to cations. Nafion not only holds

the probe molecule near the ATR surface but also functions as a cation exchange channel to promote the complexation of $Ni^{2+}$ with the DMG probe molecule.

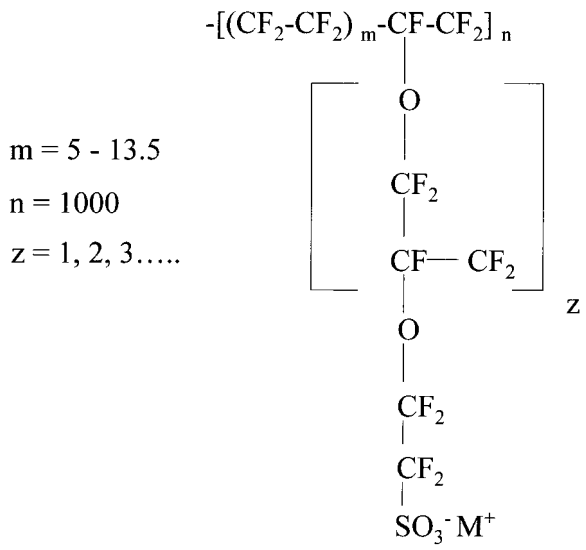


**Fig. 3.1.** Basic structure of Nafion.

DMG was chosen as the probe molecule as it is commonly used for the detection of nickel and has high selectivity toward $Ni^{2+}$ in the presence of variety of metals. The nickel dimethylglyoximate ($Ni[DMG]_2$) complex formed is very stable due to its square planar structure as seen in Fig. 3.2. Another important reason for selecting DMG is the fact that the IR spectrum of this molecule along with ($Ni[DMG]_2$) is well-established.[19-21] The C=N stretching peak at 1572 $cm^{-1}$ appears in the $Ni[DMG]_2$ spectrum, whereas it does not appear in the DMG spectrum due to intra-molecular hydrogen bonding.[22] This aspect is taken into advantage by quantifying the C=N stretching peak and thereby obtaining the amount of $Ni^{2+}$ present in the solution. $Ni^{2+}$ detection in the lake water

samples without any pre-treatments was achieved with the DMG/Nafion ATR sensor. Several limitations on the sensor performance were also noticed.

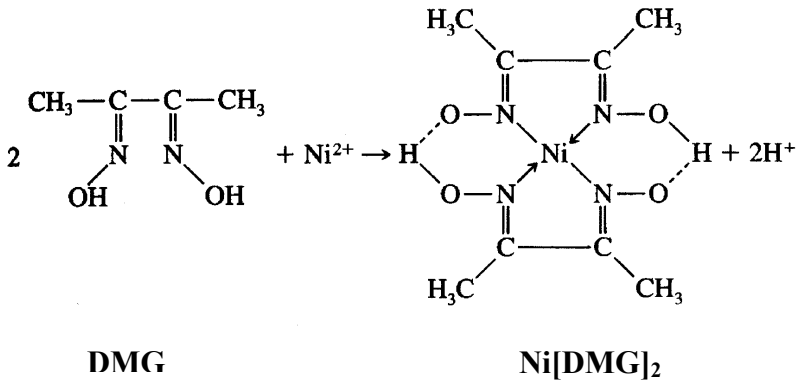


**Fig. 3.2.** Reaction governing the formation of $Ni[DMG]_2$.[23]

The data show that $Cu^{2+}$ can cause significant interference by competing with $Ni^{2+}$ for DMG probe molecules. The new infrared detection approach has a good potential to be further developed into a field sensor to locate hot spots that are highly contaminated by nickel.

## 3.2 Experimental

*Reagents and materials:* Reagent grade Dimethylglyoxime (MCB chemicals) and Nickelous sulfate (Fisher Scientific) were used. A 5 wt % solution of Nafion perfluorinated ion–exchange resin in a mixture of lower aliphatic alcohols and water was obtained from Aldrich chemicals. Reagent grade methanol, ethanol, ammonium hydroxide and hydrogen peroxide were used. Ultrapure water from a Millipore Milli-Q system (18.2 MΩcm) was utilized for all dilutions.

*$Ni^{2+}$ sample solutions:* Standard $Ni^{2+}$ solutions (pH=6) were prepared by dissolving $NiSO_{4(s)}$ in Milli-Q water. Lake water samples were collected from the Lewisville lake located north of Dallas, Texas. Lake water sample was analyzed by ICP/MS (Fisons, Model PQS).

*Silicon ATR Sensor Preparation:* The ATR parallelogram (10 x 60 x 0.7 mm, 45$^{o}$ bevel angle) was prepared from a Si(100) wafer by mechanical polishing.[24] Up to 90 internal reflections on each face with IR beam incidence normal to the bevel face could be achieved.[25] Silicon ATR crystals were cleaned in a hot organic cleaning solution $H_2O$ : $NH_4OH$ : $H_2O_2$ (5 : 1 :1), etched in HF and rinsed thoroughly with ultrapure water.[20] The sensor coating on the HF-etched silicon ATR element was prepared by dipping into a solution mixture of 0.5 wt % Nafion and 1 wt % DMG. The concentration of Nafion was adjusted by adding the appropriate amounts of stock solution (5% Nafion, Aldrich) in the DMG loading solution. A homemade dip-coating system with two pulleys and appropriate counter weight was used to ensure the uniformity of DMG/Nafion coating. The coated silicon ATR element was allowed to dry in air for 20 minutes. The bevel faces were then wiped clean with methanol prior to immersion into the $Ni^{2+}$ containing sample solution. All multiple internal reflection infrared spectroscopic (MIRIS) spectra were collected *ex-situ* after being removed from sample solution and dried in air. The reproducibility of the DMG/Nafion coating was evaluated by measuring the characteristic peak of DMG at 1365 $cm^{-1}$. The relative standard deviation was less than 6% based on the nine separate DMG/Nafion coatings. After each $Ni^{2+}$ sensing measurement, the DMG/Nafion coating was removed from silicon ATR element by immersing in a hot organics cleaning solution for 10 minutes.

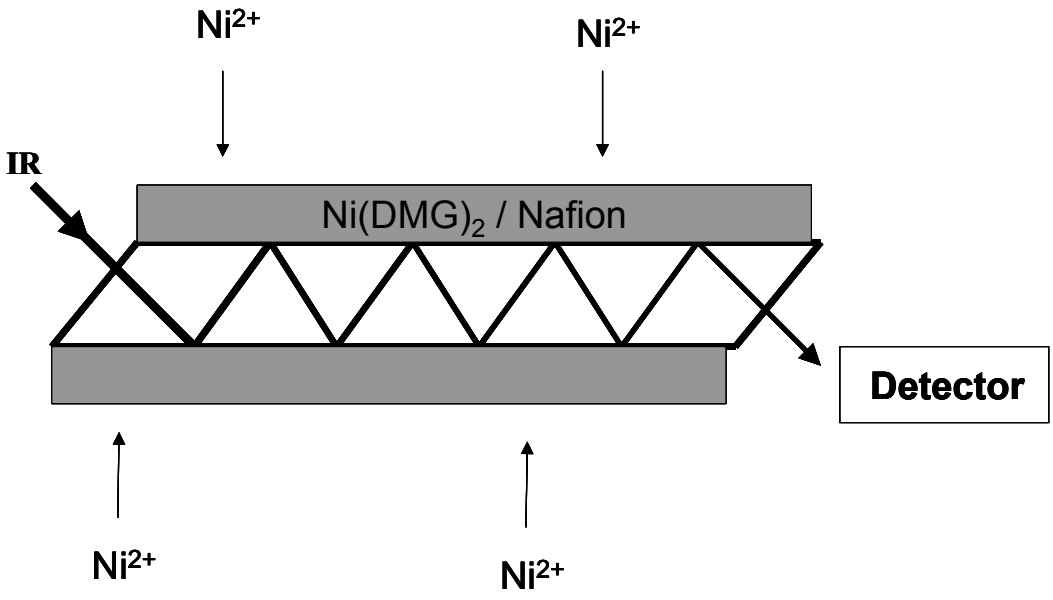


**Fig. 3.3.** Schematic for nickel IR sensor – DMG/Nafion sensing film (ca. 1.5 μm) was coated on a silicon ATR crystal (10 x 60 x 0.7 mm, 45$^{o}$ bevel angle).

*Instrumentation:* The MIRIS spectra of the silicon ATR sensor were measured using a Fourier transform infrared spectrometer (Bruker Equinox 55 FTIR system) with a MCT detector (high D*, narrow band, EG&G). A variable angle ATR accessory from Pike technologies was used to hold the ATR crystal and all spectra were measured with an angle of incidence of 45$^{o}$. All infrared (IR) spectra were collected at 4 cm$^{-1}$ resolution after averaging 200 scans under $N_2$ purge. The thickness measurements of DMG/Nafion coating were performed using cross–sectional scanning electron microscopy on a JEOL JSM-T300 electron microscope.

### 3.3. Results and Discussion

The etching of silicon substrates with HF renders the surface hydrogen terminated. The resulting silicon hydride surface is highly hydrophobic with a water contact angle larger than 65.[24] The initial approach for preparing the nickel IR sensor was to physically adsorb the DMG probe molecules directly onto the hydrophobic silicon ATR crystal surface. Fig. 3.4(a) shows the resulting MIRIS spectrum obtained from a hydrogen-terminated silicon ATR element after being dip-coated in a 1% DMG solution and dried in air.

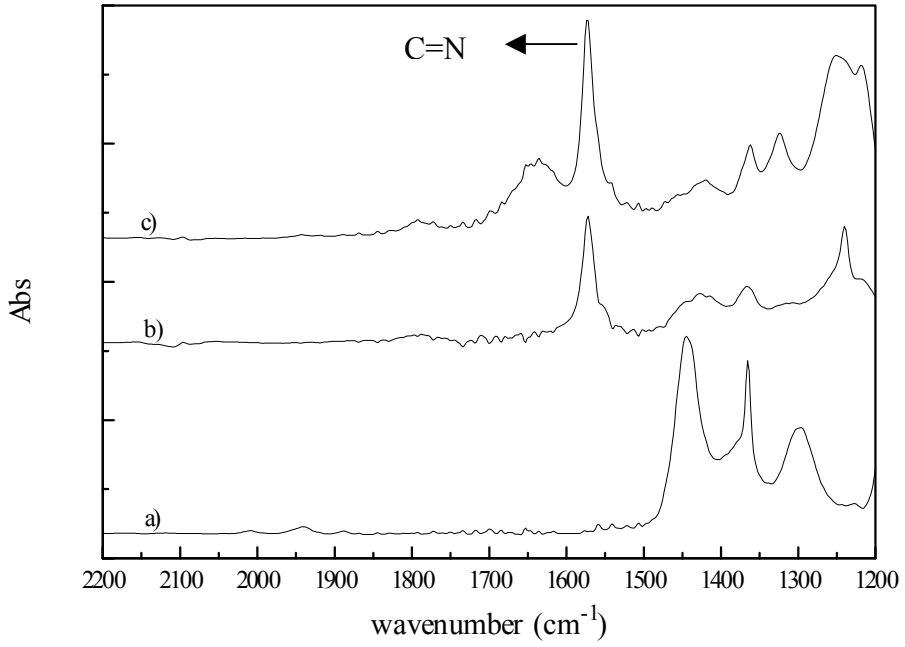


**Fig. 3.4.** MIRIS spectra of (a) Silicon ATR crystal after dip-coating in DMG solution. (b) DMG coated silicon ATR crystal after immersion in 50 ppm $Ni^{2+}$ for 10 minutes. (c) DMG/Nafion coated silicon ATR crystal after immersion in 50 ppm $Ni^{2+}$ for 10 minutes.

Fig. 3.4(b) corresponds to the MIRIS spectrum of the DMG coated silicon ATR element immersed in a 50 ppm $Ni^{2+}$solution for 10 minutes and dried in the air. The DMG spectrum is featureless in the region of 1500 – 1900 $cm^{-1}$, whereas the presence of a unique IR peak centered at the 1572 $cm^{-1}$ can be seen after exposure to $Ni^{2+}$. As illustrated in Fig. 3.4, the 1572 $cm^{-1}$ peak is attributed to the C=N stretching mode in the $Ni(DMG)_2$ complex, whereas it does not appear in the DMG spectrum due to intra-molecular hydrogen bonding.[19-22] The appearance of this unique peak in the $Ni(DMG)_2$ spectrum was employed to quantify the amount of $Ni^{2+}$ present in the solution. However, it was also noticed that the DMG coating was not uniform and easily detached from the silicon ATR crystal surface. These results indicated the need for a suitable matrix to hold the probe molecule and to ensure a uniform and reproducible coating.

### 3.3.1 Matrix factor

Nafion is a perfluorinated cation exchange polymer with $SO_3^-$ pendant groups attached to its fluoropolymer chains. The fluorocarbon polymer backbone of Nafion should adhere well on the hydrophobic silicon ATR surface. The IR spectrum of Nafion has been well-studied.[26-29] In addition, the cation exchange properties of Nafion membranes should assist in transporting $Ni^{2+}$ ions into the matrix to interact more efficiently with the DMG probe molecule. Figure 3.4(c) shows an *ex situ* MIRIS spectrum of a DMG/Nafion coated ATR element after being immersed in a 50 ppm $Ni^{2+}$ solution. The dip-coating solution used to prepare the ATR element was a mixture of 1% DMG/ 0.5% Nafion. The $Ni(DMG)_2$ spectrum obtained for a DMG/Nafion coated ATR element shows a ca. 40% increase in the C=N stretching peak intensity as compared to

just a DMG coated element, ref. Fig. 3.4. (b) and 3.4.(c). More importantly, the Nafion coating was visibly uniform and proven to be quite robust in aqueous environments as determined from subsequent experiments. The reproducibility of the DMG/Nafion coating is better than 6% RSD as evaluated by its characteristic DMG peak at 1365 $cm^{-1}$. Further it was seen that Nafion did not cause any shift in the characteristic peak positions of $Ni(DMG)_2$, although there was a slight overlap of a Nafion peak (i.e. solvated $SO_3^-$ group in the 1600 – 1650 $cm^{-1}$) with that of the C=N peak from $Ni(DMG)_2$. The results suggest that Nafion film aids in holding the DMG probe molecule onto the silicon ATR element and can be used as a matrix.

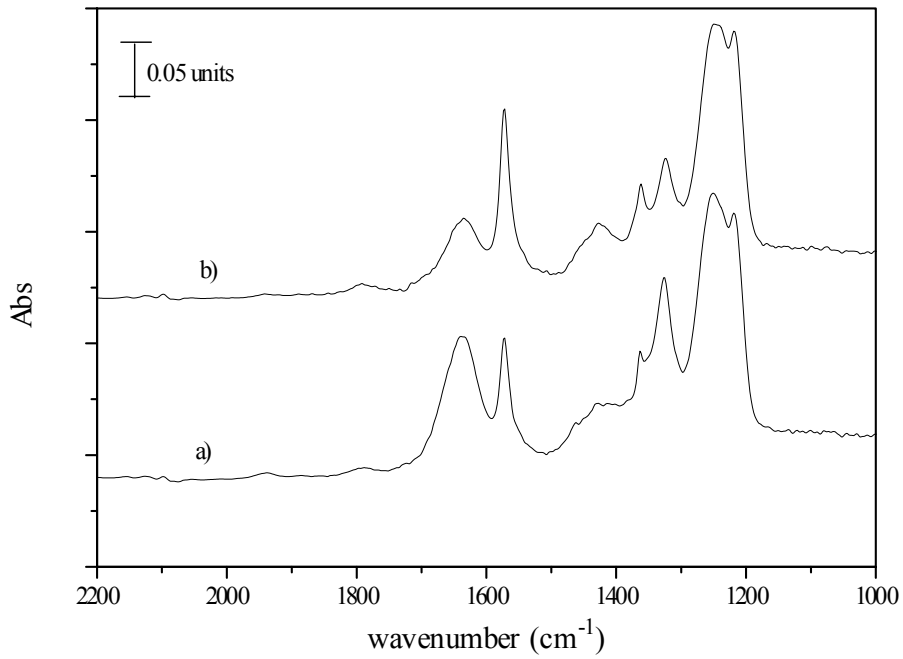


**Fig. 3.5.** IR spectra of (a) 1 % Nafion / 1 % DMG coated crystal dipped in 30 ppm $Ni^{2+}$ (b) 0.5 % Nafion / 1 % DMG coated crystal dipped in 30 ppm $Ni^{2+}$.

To optimize the nickel IR sensor performance, the Nafion concentration (0.1%, 0.5% and 1%) in the dip-coating solution was varied, while fixing the DMG loading at 1% in all cases. It was noticed that for the lowest concentration of Nafion (0.1%), the coating on silicon ATR crystal was non-uniform based on observation under SEM. Thus the analysis was confined to 0.5% and 1% Nafion concentrations. The C=N peak height for 0.5% Nafion was found to be significantly larger than for the 1% case under similar conditions as can be seen in Fig. 3.5. Several factors could have contributed to the lower detectable C=N peak height in the thicker film prepared from 1% Nafion coating solution. For example, the limited penetration depth of the IR evanescent wave could hamper the $Ni^{2+}$ detection in the thicker Nafion film.

To determine the penetration depth, a reported refractive index of general fluoropolymers was used [32] to approximate the actual refractive index of DMG/Nafion films. The penetration depth of the evanescent wave in Nafion film for 1572 $cm^{-1}$ radiation (corresponding to C=N stretching mode) was estimated to be less than 0.5 μm.[25] I further measured the thickness of our DMG/Nafion coating using cross–sectional SEM. It was found that the average thickness for films prepared from 0.5% and 1% Nafion solutions was 1.5 and 2.6 μm respectively. The obtained data suggested that not all of the DMG/Nafion film could be seen by the IR evanescent wave at 1572 $cm^{-1}$ (corresponding to C=N stretching peak). Therefore, an assimilation process of $Ni^{2+}$ ions from the solution into the detectable DMG/Nafion region near the ATR surface is needed prior to nickel detection. Consequently, a thicker coating will result in a weaker observable C=N peak since a longer assimilation time (*via infra*) will be needed to transport $Ni^{2+}$ through a thicker Nafion matrix.

In addition, the IR absorption peak in the 1600-1650 $cm^{-1}$ which corresponds to the $SO_3^-$ group of Nafion background is significantly enhanced in the 1% Nafion case as compared to the 0.5% case.[27, 28] The $SO_3^-$ background peak partially overlaps with the edge of C=N peak from $Ni(DMG)_2$ complex. Based on the above considerations, the concentration of Nafion in the dip-coating solution was chosen to be 0.5%.

### 3.3.2 Sampling time factor

A systematic study was undertaken to determine the optimum sampling time of nickel IR sensor. Fig. 3.6 depicts the time dependent C=N peak intensity data obtained from a nickel IR sensor dipped in 30 ppm of $Ni^{2+}$ solution.

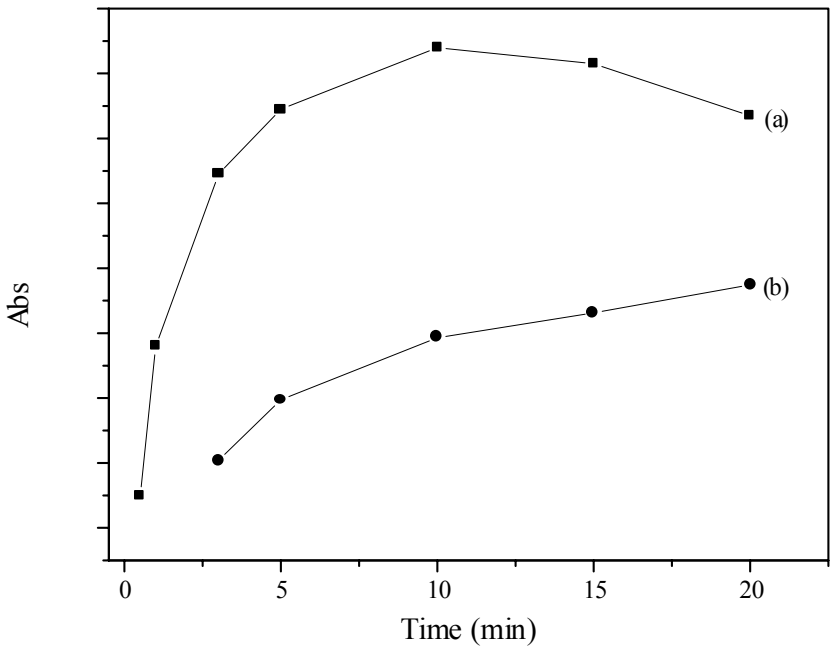


**Fig. 3.6.** Nickel IR sensor response vs. immersion time in 30 ppm $Ni^{2+}$ solution for coating containing (a) 0.5 % and (b) 1% Nafion.

With the increase in immersion time it was observed that the peak intensity showed a noticeable increase. In the case of 0.5% Nafion the C=N peak intensity reached a maximum at 10 minutes, followed by a slight decrease. One can attribute the intensity decrease to the slight leaching of the $Ni(DMG)_2$ from the Nafion matrix into the solution. 10 min was selected as the optimum sampling time since it was the minimum immersion time required to provide the largest value for the observed C=N peak intensity. The assimilation of the $Ni^{2+}$ analyte takes longer as expected in the thicker coating prepared from 1% Nafion coating solution. The C=N peak intensity was found to increase steadily with time but was consistently less than its 0.5% Nafion counterpart within 20 minutes of testing. The IR sensor response beyond 20 minutes was not examined since the extended sampling time would impede the practical utilization of the sensor.

### 3.3.3. Optimization of DMG concentration

Next the DMG concentration in the coating solution was optimized to maximize the sensing capacity of the nickel IR sensor. A progressive increase in the intensity of the C=N peak was observed with the increase of DMG concentration in the coating solution. However, an excess leaching of the red $Ni(DMG)_2$ complex from the nickel IR sensor was observed when the sensing film was prepared in the coating solution with the DMG concentration exceeded 1%. The leaching of $Ni(DMG)_2$ can affect the reproducibility and detection sensitivity of the nickel IR sensor. In addition, no further improvement of $Ni^{+2}$ detection limit was observed when the DMG concentration exceeded 1%. The concentration of 1% DMG in 0.5% Nafion coating solution was chosen to prepare the nickel IR sensor for the subsequent sensor work.

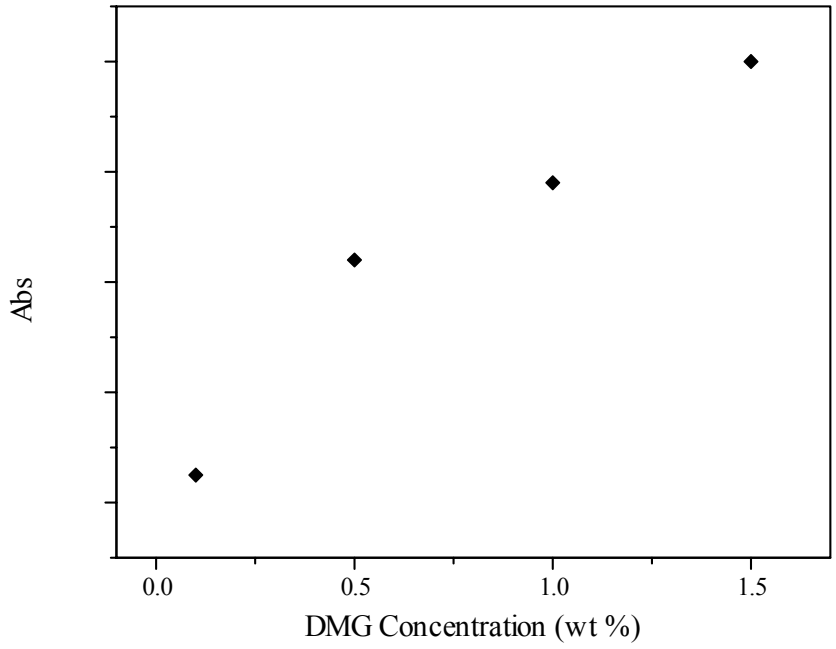


**Fig. 3.7**. IR sensor response for varying DMG concentrations.

### 3.3.4. Quantitative Analysis

Fig. 3.8 shows the MIRIS spectra obtained from a nickel IR sensor immersed in the sample solutions of different $Ni^{2+}$ concentration. There is a progressive increase in the C=N peak height with the increase of the $Ni^{2+}$analyte. Apart from the observed increase of C=N peak intensities, the rest of the background spectra look similar proving the uniformity and reproducibility of the DMG/Nafion coating on the silicon ATR element. As the C=N peak partially overlaps with the solvated $SO_3^-$ peak from the Nafion matrix, a curve fitting calculation based on the Levenberg–Marquardt algorithm was employed as to separate the C=N peak from its Nafion background. For comparison, direct measurement of the C=N peak height after interactively fixing the baseline from 1510 $cm^{-1}$ – 1690 $cm^{-1}$ was also carried out.

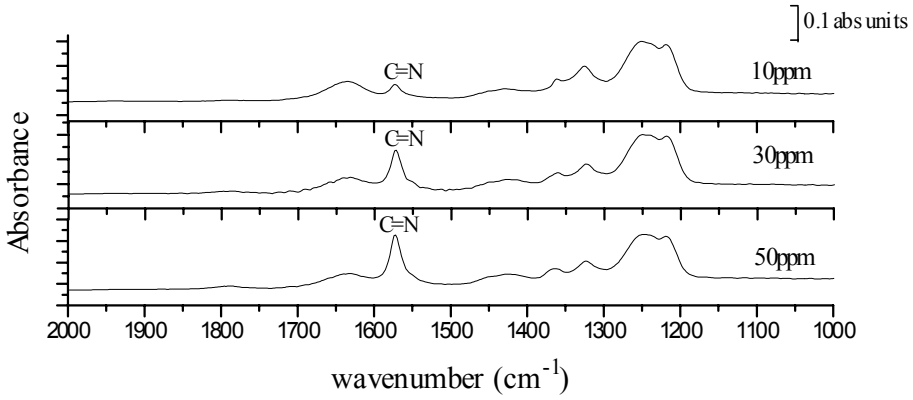


**Fig. 3.8.** MIRIS spectra of a nickel IR sensor after immersing in 10-50 ppm $Ni^{2+}$ solutions. New DMG/Nafion coating was used for each measurement.

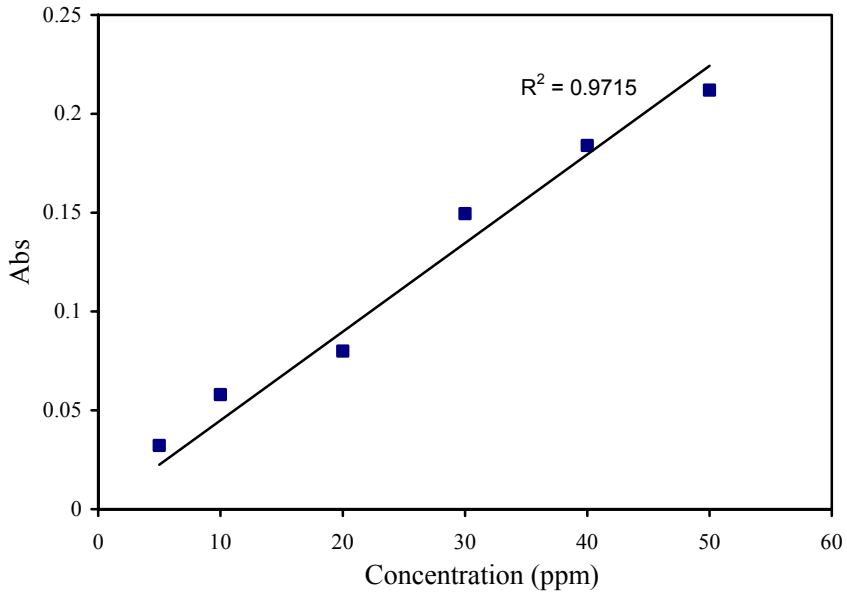


**Fig. 3.9.** Calibration for the IR sensor in the concentration range of 5 – 50 ppm at pH= 6.

The results obtained using curve fitting were within 4% of the results obtained by measuring the peak height directly. Hence, it was deemed appropriate to use results obtained directly from C=N peak height without any mathematical manipulation

A fairly linear fit was obtained with a $R^2$ value of 0.97 based on three runs, and the precision was found to be satisfactory with an RSD < 6% for the three runs. The detection limit of the nickel IR sensor, based on C=N signal which is substantially greater than the blank (S/N >3 as compared to the blank), was determined to be 5 ppm at pH=6.

### 3.3.5. pH factor

The complexation of $Ni^{2+}$ with DMG is usually carried out in a slightly alkaline medium, since the formation of $Ni(DMG)_2$ is accompanied by the loss of two protons (Fig. 3.2).

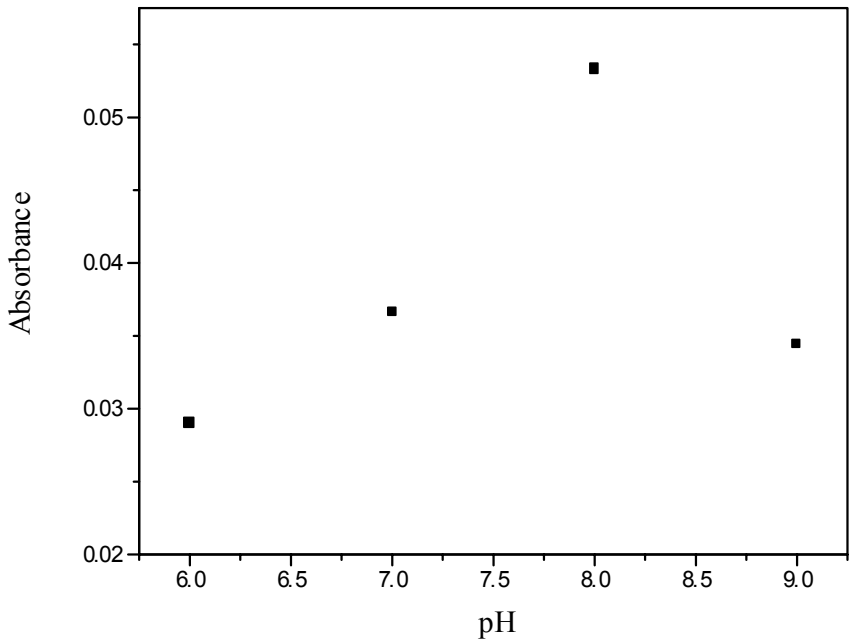


**Fig. 3.10.** IR sensor response in 5 ppm $Ni^{2+}$ under different pH conditions.

To determine a suitable pH range for the nickel sensing operation, nickel IR sensor responses in 5 ppm $Ni^{2+}$ solutions of different pH was investigated. The experimental data indicated that the C=N peak intensity increases with the increase of solution alkalinity with a pH range of 5 to 8. A substantial drop in the C=N peak absorbance value at pH ≥ 9 was observed due to the leaching of red $Ni(DMG)_2$ out of the matrix. The nickel detection at lower pH was also hampered, because the formation of $Ni(DMG)_2$ complex is not thermodynamically favorable in more acidic conditions. A point worth mentioning is that the detection limit of the IR sensor can be further improved to 1 ppm $Ni^{2+}$in a slightly alkaline solution (pH = 8). Therefore, the operational pH range for the DMG/Nafion $Ni^{+2}$ sensor should be kept within 6-8 to improve nickel detection.

### 3.3.6. Interference

It is known that $Pd^{2+}$, $Pt^{2+}$, $Co^{2+}$, $Cu^{2+}$ and $Fe^{2+}$ ions also form complexes with DMG with differing stabilities. As Pd and Pt are rather rare in nature, our investigation was confined to the $Co^{2+}$, $Cu^{2+}$ and $Fe^{2+}$ ions. Fig. 3.11 shows the effect of these three ions on the IR sensor responses to 30 ppm $Ni^{2+}$. The vertical axis corresponds to the C=N peak intensity ratio obtained with/without the presence of the $Co^{2+}$, $Cu^{2+}$ and $Fe^{2+}$ ions. The intensity ratio should ideally be one, if no interference occurs. In the presence of $Co^{2+}$ and $Fe^{2+}$, the nickel IR sensor responds optimally with a slight deviation from a straight line, which is close to the experimental error margin. In the case of $Cu^{2+}$ there is a continual drop in the C=N peak intensity with the increase of $Cu^{2+}$ concentration. However, the C=N peak intensity corresponding to $Ni(DMG)_2$ is still prominent even

when 30 ppm of $Cu^{2+}$ is present along with 30 ppm of $Ni^{2+}$. This observation suggests that $Cu^{2+}$ can actively compete with $Ni^{2+}$ to occupy the DMG binding sites in Nafion matrix.

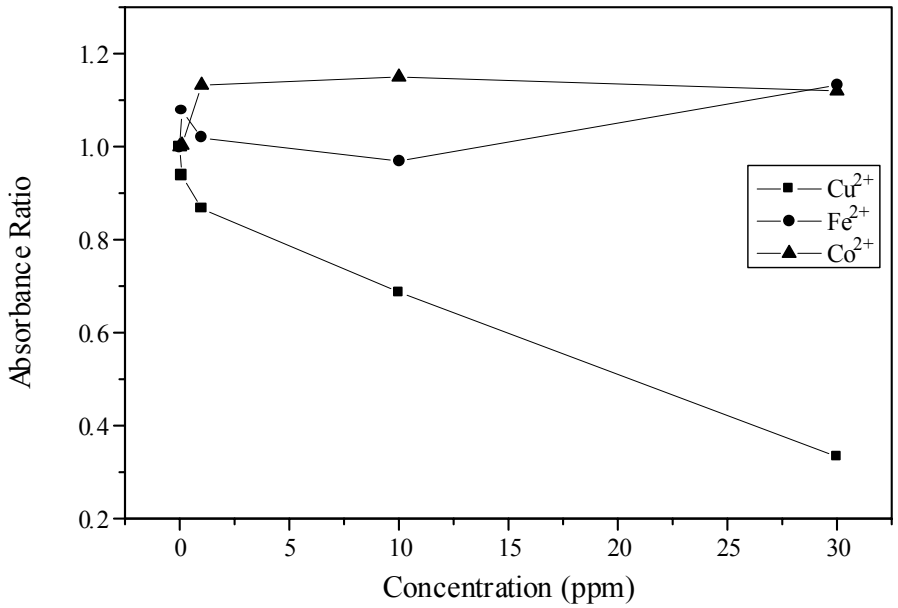


**Fig. 3.11.** Nickel IR sensor responses to 30 ppm $Ni^{2+}$ in the presence of $Co^{2+}$, $Cu^{2+}$ and $Fe^{2+}$ ions of increasing concentration. The absorbance ratio corresponds to C=N peak intensity ratio without/with other interfering ions.

The formation constant K for $Cu(DMG)_2$ is 12, while that for $Ni(DMG)_2$ is 11.16 indicating that indeed Cu is an active competitor for the DMG sites.[31] It is noteworthy that $Cu(DMG)_2$ has its C=N peak location at 1560$cm^{-1}$, which is different from that of $Ni(DMG)_2$ complex. Though the nickel IR sensor did not respond optimally in the presence of $Cu^{2+}$, it could still be used to qualitatively identify $Cu^{2+}$ at higher concentrations based on the different C=N peak location for $Ni(DMG)_2$ and $Cu(DMG)_2$.

### 3.3.7. Nickel analysis in natural water system

To test the effectiveness of the sensor experiments using lake water samples were carried out. The lake water did not contain any detectable amounts of $Ni^{2+}$ but contained other ions such as Zn, Ca, Sr, K, B, Si, Mg, Na, which were in the ppm range based on ICP- MS analysis. Appropriate amounts of standard $Ni^{2+}$ solution were added to both samples to make up for 10 ppm $Ni^{2+}$. The pH of the pure water sample was adjusted appropriately to match the lake water pH value, i.e. about 7.

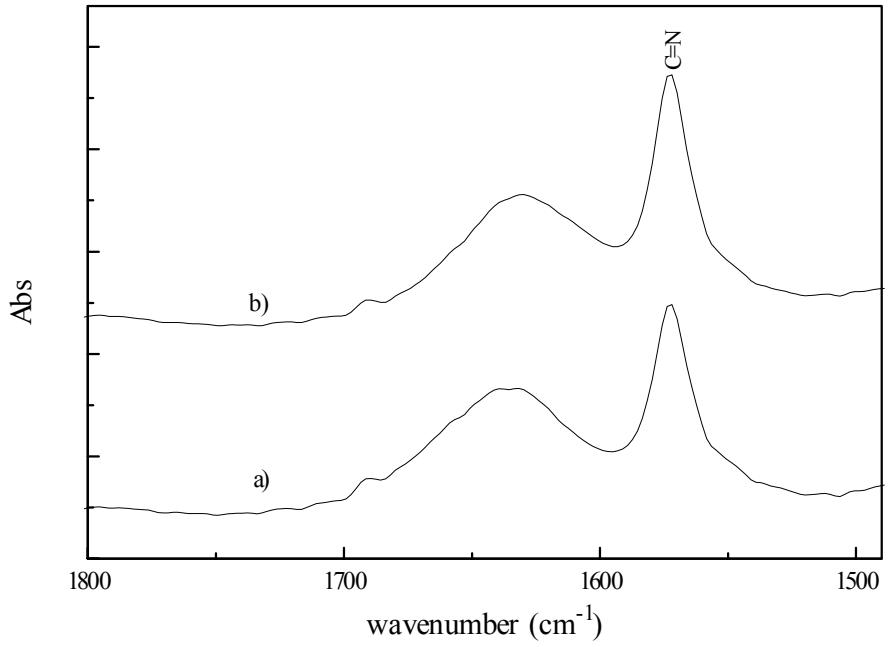


**Fig. 3.12.** IR sensor response in (a) 10 ppm $Ni^{2+}$ / UPW and 10 ppm $Ni^{2+}$ / Lake water.

The C=N peak intensity of 10 ppm $Ni^{2+}$detected in the lake water was found to be similar to that of the laboratory water. It is important to note that pre-treatments (like

filtration, precipitation etc.) were not needed for the detection of 10 ppm $Ni^{2+}$ in the lake water sample using our nickel IR sensor. Organic residues and colloidal suspensions resulting from natural decay process of vegetation and aquatic species are known to exist in ppm range in natural waters. The fact that no apparent decrease or interference in the C=N peak intensity occurs, inspite of the presence of natural organic background, suggests the potential utilization of the nickel IR sensor in the field applications.

We attribute the fluorocarbon polymer backbone of the Nafion coating for the effective blockage of the organic interference from reaching the silicon ATR surface, while the $Ni^{2+}$ ions in the solution were allowed to assimilate in by Nafion's cation exchange function and detected by the embedded DMG probe molecules.

In summary, a new nickel detection method based on DMG probes embedded in Nafion matrix was demonstrated using FTIR–ATR technique. The limit of $Ni^{2+}$ detection based on the unique C=N peak in $Ni(DMG)_2$ was determined to be 1-5 ppm in the pH operation range 6-8. The sensor response seems to be unaffected by the presence of a majority of other metal cations except $Cu^{2+}$. Direct nickel detection in natural water samples without sample pretreatments was demonstrated. The nickel IR sensor can be used in conjunction with a portable FTIR spectrometer to probe hot spots contaminated with high ppm of $Ni^{2+}$. In order to make the IR sensor more robust, further improvements need to be made with regards to lower detection limits and regeneration of the sensor. The possibility of modifying the silicon surface using organic molecules has been shown by a number of researchers and characterized using IR spectroscopy.[32,33] We are currently looking into the different synthetic pathways to covalently attach organic probe

molecules onto the silicon ATR surface in order to improve the sensor's effectiveness and to implement similar approaches to detect other metals as well.

### 3.4. Chapter References


1. J. O. Nriagu and J.B. Sprague. Cadmium in the Aquatic Environment. A Wiley – Interscience publication, N.Y. (1987).
2. J. O. Nriagu and E. Niebor. Chromium in the Natural and Human Environment. A Wiley - Interscience Publication, N.Y. (1988).
3. C. L. Lewis, W. L. Ott and N. M. Sine. Analysis of Nickel, Pergamon Press Inc., Oxford, (1966).
4. C. L. Lewis and W. L. Ott. Analytical Chemistry of Nickel. Pergamon Press, Oxford, (1970).
5. V. M. Peshkova and V. M. Savastina. Analytical Chemistry of Nickel. Israel Program for Sceintific Translations, (1967).
6. K. Toei, S. Motomizu and S. Kuse. *Anal. Chimi. Acta*., **75**, 323 (1975).
7. J. Wang, V. B. Nascimento, J. Lu, D. S. Park and L. Agnes. *Electroanalysis,* **8**, 635 (1996).
8. J. Wang, P. V. A. Pamidi, V. B. Nascimento and L. Agnes. *Electroanalysis*, **9**, 689 (1997).
9. R. P. Baldwin, J. K. Christensen and L. Kruger. *Anal. Chem.*, **58**, 1790 (1986).
10. J. M. Zen and M. L. Lee. *Anal. Chem*, **65**, 3238 (1993).
11. J. S. Jeon, R. P. Sperline, and S. Raghavan. *Appl. Spectrosc.*, **46**, 1644 (1992).

12. V. B. Maurel, C. Vallat and D. Goffinet. *Appl. Spectrosc.,* **49**, 556 (1995).

13. V. B. Maurel, C. Vallat and D. Goffinet. *Appl. Spectrosc.*, **49**, 563 (1995).

14. J. Chen and J. A. Gardella. *Appl. Spectrosc.*, **52**, 361 (1998). DeGrandpre, M. D. Burgess, L. W.; White, P. L. and Goldman, D. S. *Anal. Chem*., **62**, 2012 (1990).

15. Yang, L. and Saavedra, S. *Anal. Chem*., **67**, 1307 (1995).

16. M. C. Lamontagne, K. A. Parthum, W. Rudolph Seitz and S. A. Tomellini. *Appl. Spectrosc.*, **48**, 1539 (1994).

17. F. Reagan, M. Meaney, J. G. Vos, B. D. MacCraith and J. E. Walsh. *Anal. Chim. Acta.,* **334**, 85 (1996).

18. (a) O. Chyan, J. J. Chen, F. Xu and J. J. Wu. *Anal. Chem.*, 69, 2434 (1997). (b) J. J. Chen, F. Xu, T. Ponnuswamy, R. Chan, J. J. Wu, A. Prasad and O. Chyan. *Recent Res. Devel. Applied Spectroscopy*, **3**, 81 (2000).

19. R. Blinc and D. Hadzi. *J. Chem. Soc.,* 4536 (1958).

20. A.Bigotto, G. Costa, V. Galasso and G. De Alti., *Spectrochii. Acta.***, 26A**, 1939 (1970).

21. A. Bigoto, V. Galasso and G. De Alti, *Spectrochimi. Acta.*, **27A**, 1659 (1971).

22. P. K. Panja, S. Bala, C. Pal and P. N. Ghosh. *J. Mol. Str.* **249**, 277 (1991).

23. D. A. Skoog, D. M. West and F. J. Holler, Fundamentals of Analytical Chemistry, Saunders Colege Publishing, 88, Sixth Edition, FL. (1997).

24. O.M.R. Chyan, J. J. Chen and J. J. Wu. *Appl. Spectrosc.*, **51**, 1901 (1997).

25. N. J. Harrick. Internal Reflection Spectroscopy, Interscience Publishers: N.Y., 1967.

26. M. Falk. *Can. J. Chem.*, **58**, 1495 (1980).

27. S. Quezado, J. C. T. Kwak and M. Falk, *Can. J. Chem.*, **62**, 958 (1984).

28. C. H. Weigner, *Polymer*, **20**, 371 (1979).

29. I. Palinko, B. Torok, G.K. Surya and G. A. Olah. *Appl. Catal. B.,* , **174**, 147 (1998).

30. J. Brandrup, E. H. Imergut, E. A. Grulke. Handbook of Polymers. Wiley – Interscience publication: N.Y., 1998.

31. J.A. Dean, Lange's Handbook of Chemistry, 13th Edition, McGraw Hill Inc. (1972).

32. H. Liu and R.J. Hamers, *J. Am. Chem. Soc.*, 119, 7593 (1997).

33. W.F. Bergerson, J.A. Mulder, R.P. Hsung and X.Y. Zhu, *J. Am. Chem. Soc*., **121**, 454 (1999).

# CHAPTER 4

# STUDY OF THE INTERACTION OF HYDROGEN TERMINATED SILICON(100) UNDER DIFFERENT ENVIRONMENTS

## 4.1. Introduction

During the course of fabricating IC devices, the silicon surface undergoes various chemical treatments multiple number of times. In order to produce defect free devices it is imperative to maintain a clean and stable silicon surface between the numerous processes that are involved. One of the critical processes involves etching with HF solutions to remove native or chemical oxide to obtain a hydrogen-terminated surface. The hydrogen-terminated surface is stable against air oxidation for long durations of time and is of great importance in the whole fabrication sequence. Due to the importance of this phenomenon, several workers have studied the factors that lead to the oxidation of the such surfaces in different environments.[1-4] A number of studies have been carried out to study the effect of exposing hydrogen terminated silicon in air and UPW. Morita *et al.* were one of the first to study the effect of immersing Si(100) substrates in UPW.[2] They characterized the oxidation based on the thickness of the oxide that was formed. Boonekamp *et al.* studied the effect of immersing Si(111) in UPW using ATR – FTIR spectroscopy and used a Ge prism as an internal reflection element.[4] Niwano *et al.* used FTIR – ATR to observe the effect of immersing H-Si(100) in UPW under ambient conditions and concluded that there was a hydrogen exchange reaction between the H-Si(100) surface and water.[5] A number of workers have looked at the oxidation

mechanism in UPW under UHV conditions and by using theoretical calculations.[6-8] They characterized the effect of oxidation by measuring the thickness of native oxide that grew with time and by using spectroscopic techniques to deduce the mechanism. Weldon *et al.* studied the effect of exposing H – terminated Si(100) [H-Si(100)] to water molecules at UHV and concluded that the Si – Si dimer bond is the target for initial insertion of an O atom during the early stages of oxidation.[6] Oxidation of H-Si(100) in air has been studied in detail by Niwano *et al.* where they have depicted the different stages of oxidation of the substrate. They studied the effect of humidity in air toward oxidation of H-Si(100) surfaces.[9] This chapter deals with the interaction of H-Si(100) when immersed in HF, metal / HF, UPW, metal / UPW and UPW with varied amounts of dissolved oxygen concentrations. FTIR – ATR was used to study the change in the different modes of vibration when the silicon surface comes in contact with the above-mentioned systems. This technique gives detailed information on the change in vibrational modes of the silicon hydride in different environments and thereby throws light on the mechanistic aspects that lead to such changes. The focus of this study is to determine the vibrational changes that a H–Si(100) surface undergoes in the initial stages when it comes in contact with the different environments.

## 4.2. Experimental

Reagents and materials: Electronic grade HF, HCl, $H_2O_2$, $NH_4OH$ were used for treating the silicon surface. Ultra-pure water ($R > 18.2\ M\Omega cm^{-1}$) was used for rinsing and immersing the silicon ATR element for all experiments. The PFA (polyfluoroalkoxy)lab-ware used in this study was pre-cleaned by boiling in 10% $HNO_3$ thrice followed by a

ultra-pure water rinse.

Silicon ATR Sensor Preparation*:* Si(100) double polished wafer with a resistivity of 0.6-1.0 ohms.cm was used to prepare the ATR parallelogram (10 x 60 x 0.7 mm, $45^o$ bevel angle). Up to 86 internal reflections on each face with IR beam incidence normal to the bevel face could be achieved. The Silicon ATR crystal was cleaned in a hot organic cleaning solution $H_2O : NH_4OH : H_2O_2$ (1 : 1 :5), etched in HF and rinsed thoroughly with ultra pure water.

Instrumentation: The MIRIS spectra of the silicon ATR crystal were measured using a Fourier transform infrared spectrometer (Bruker Equinox 55 FTIR system) with a MCT detector (high D*, narrow band, EG&G). A variable angle ATR accessory from Pike technologies was used to hold the ATR crystal and all spectra were measured with an angle of incidence of $45^o$. All infrared (IR) spectra were collected *ex-situ* at 2 $cm^{-1}$ resolution after averaging 200 scans under $N_2$ purge.

Experimental setup to study effect of dissolved oxygen*:* To study the effect of dissolved oxygen, experiments were conducted under controlled conditions. Fig. 4.1. depicts a schematic for the setup used during the study. The glove box, model 855 – AC by Plas – Labs Inc. was used for these experiments. The atmospheric oxygen concentration in the glove box atmosphere was ~21% when exposed to the surroundings. In order to carry out the experiments under controlled conditions these levels were brought to <1% prior to the start of each experiment by insulating the glove box from its surroundings and purging with $N_2$. This process of pumping out air followed by flooding in with $N_2$ was carried out

until the oxygen level was within the acceptable limits. The atmospheric oxygen level was measured using Model 1630 oxygen meter by Kern Company Instruments Inc.

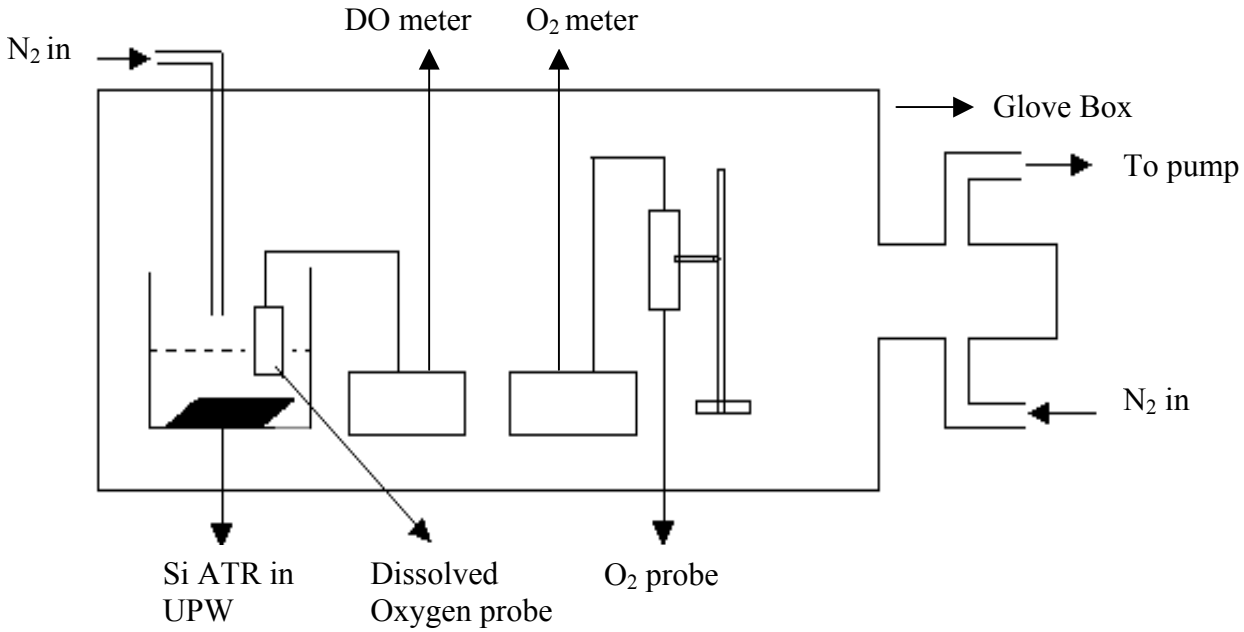


**Fig. 4.1.** Schematic depicting the set up used for studying the effect of dissolved oxygen on H-Si(100) surfaces.

The probe constituted a galvanic electrode capable of measuring 0 – 100% atmospheric oxygen. In order to measure the dissolved oxygen (DO) in UPW, a DO analyzer (DO-166) from Lazar Laboratories inc. was used. The DO probe was connected to a high input impedance potentiometer (Accumet 50 Fisher Scientific) and the voltage reading obtained was correlated to the DO concentration. The DO probe was capable of detecting 0 – 20 ppm dissolved oxygen with a detection sensitivity of 10 – 15 ppb. The beaker containing UPW was bubbled with $N_2$ along with the purging of the glove box in which it was placed. The dissolved oxygen level in UPW can be maintained for several

days using this setup.

### 4.3. Results and Discussion

Fig. 4.2 depicts a H-Si(100) ATR spectrum obtained after HF treatment. The prominent peaks pertaining to the dihydrides are the symmetric ($D_1$) and the asymmetric ($D_2$) stretching peaks. The Si(100) crystal has a square lattice wherein each silicon atom at the uppermost layer has two dangling bonds.[10] The presence of these dangling bonds renders the surface reactive , thus capping these bonds with hydrogen atoms passivates the surface. Due to the presence of two hydrogen atoms for each silicon atom, only the dihydride stretching modes should be observed under ideal conditions.

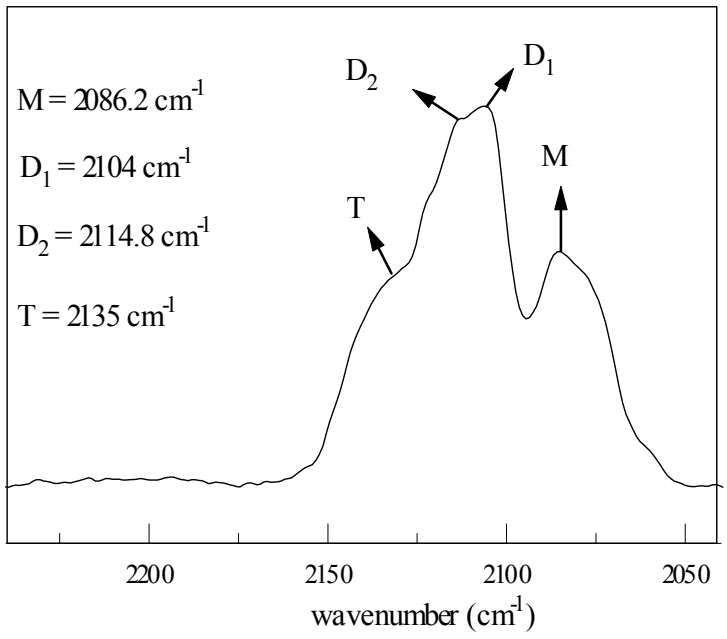


**Fig. 4.2.** Si(100) spectrum obtained after immersion in 4.9% HF for 5 minutes.

The spectrum reflects a different scenario, namely the presence of monohydride (M) and trihydride (T) peaks indicating a certain degree of surface micro-roughness. The initial study was concerned with the effect of metal contaminants in HF on the H-Si(100) silicon surface. Thus a baseline study corresponding to immersion of the Si ATR crystal in pure HF was carried out.

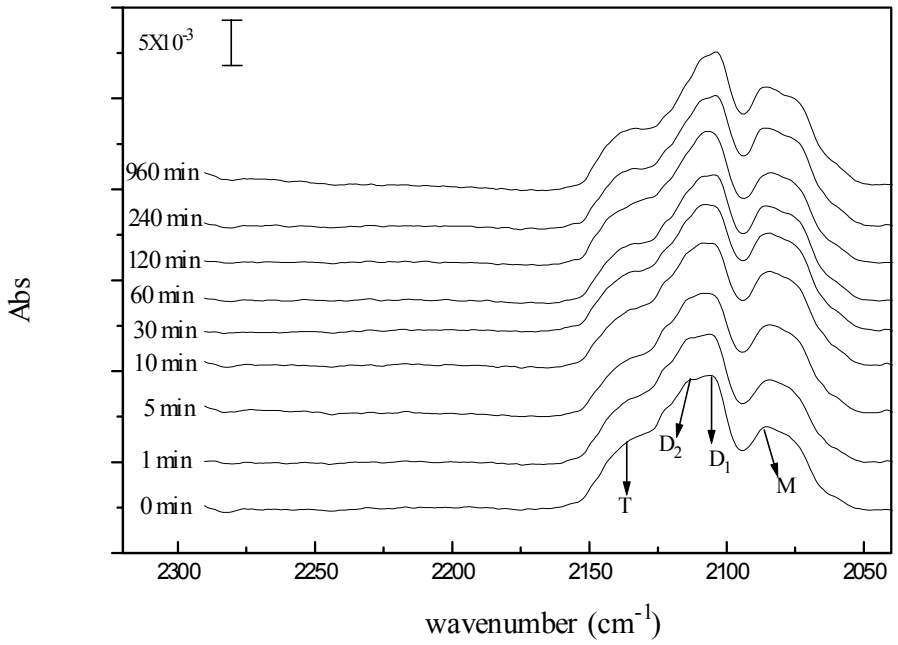


**Fig. 4.3.** Time dependent spectra of H-Si(100) surface immersed in HF for different durations of time.

Based on Fig. 4.3, one can observe minor changes in the spectra with increase in the immersion time. Fig. 4.5 depicts the integrated peak intensity of H-Si(100) where Si-$H_2$ and Si-H denote dihydride and monohydride peaks respectively. It appears that the dihydride peak initially decreases along with an increase in the monohydride peak in the first few minutes. At the end of 120 min there seems to be a sharp drop in the

monohydride peak intensity after which it tends to increase once again. It seems to appear that the trihydride peak ( 2135 $cm^{-1}$) becomes more pronounced with the passage of time. One could possibly correlate the drop in the monohydride peak after 120 min to the advent of the trihydride peak, as both peaks are representative of Si(111) facet formation. The small increase in the monohydride and trihydride peak indicates that the surface undergoes morphological change during the course of immersion in HF solutions.

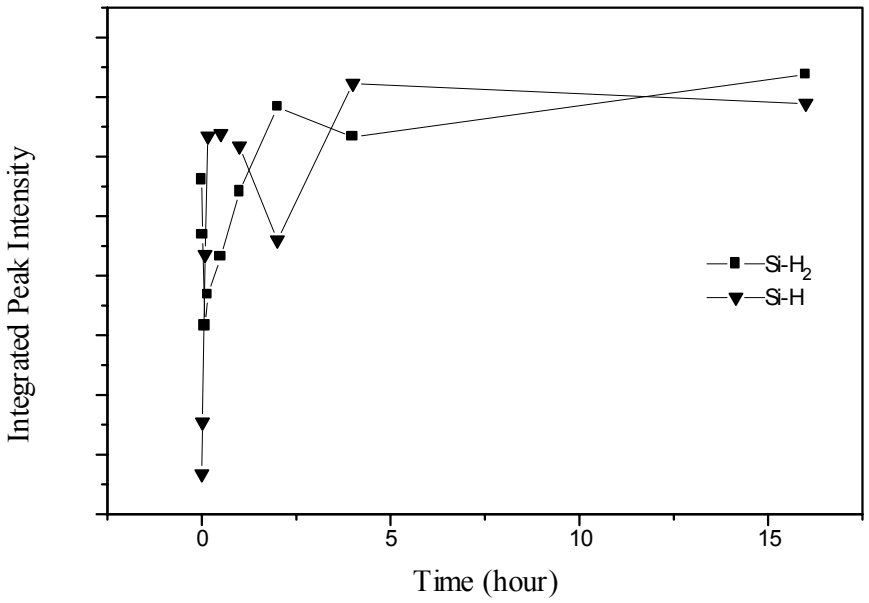


**Fig. 4.5.** Integrated peak intensity of H-Si(100) immersed in 4.9% HF for different durations of time.

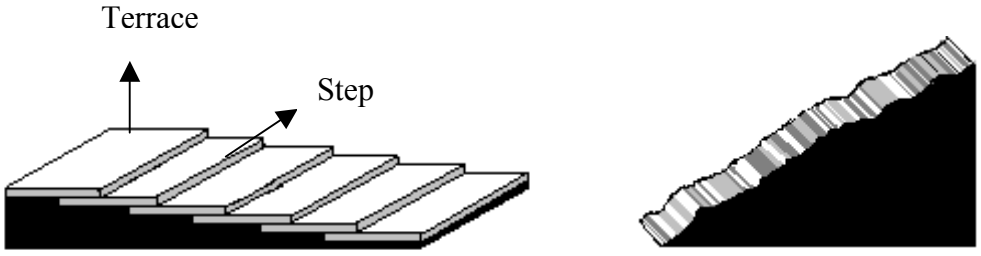


(a) (b)

**Fig. 4.4.** Schematic depicting (a) perfect surface (b) rough silicon surface.

Fig. 4.4 is an illustration of a perfect and rough silicon surface. The terrace structure represents a smooth surface containing the dihydride hydride species, while the steps indicate the monohydride state. The trihydrides are located in the kinks, which are the step edges. Fig. 4.4(b) depicts a surface with large scale micro-roughness which corresponds to the formation of (111) facets in the case of Si(100) substrates. The increase in surface micro-roughness would indicate an increase in the step surface area.

Etching of crystalline silicon surfaces in HF solutions has been studied by Willeke *et al.* where they observed etch pit formation when the substrates were immersed for long durations of time.[11] They studied samples that had been immersed in HF for over 100 days and determined the etch rate to be as low as $4 \times 10^{-3}$ Å / min. In our case it is highly unlikely that any pits could have been formed as the samples under consideration were immersed for less than a day. Based on the data, namely the increase in the (111) facets one can say that the surface roughness for the (100) sample increases when it is immersed in HF for longer periods of time.

Fig. 4.6 represents the time dependent spectra of H-Si(100) in 4.9% HF containing 10 ppb of $Cu^{2+}$. One can see a more dramatic change in the shape of the hydride peak with time. The increase in the monohydride and trihydride peaks is clearly evident at the end of 10 min. The shape of the peaks undergoes drastic changes after 120 min by the dominance of the monohydride peak. These observations become clear when one looks at Fig. 4.7, which is obtained after integrating the dihydride and monohydride peaks. There is a monotonic increase in the monohydride peak along with a corresponding decrease in the dihydride peak indicating an obvious change in the surface

morphology.

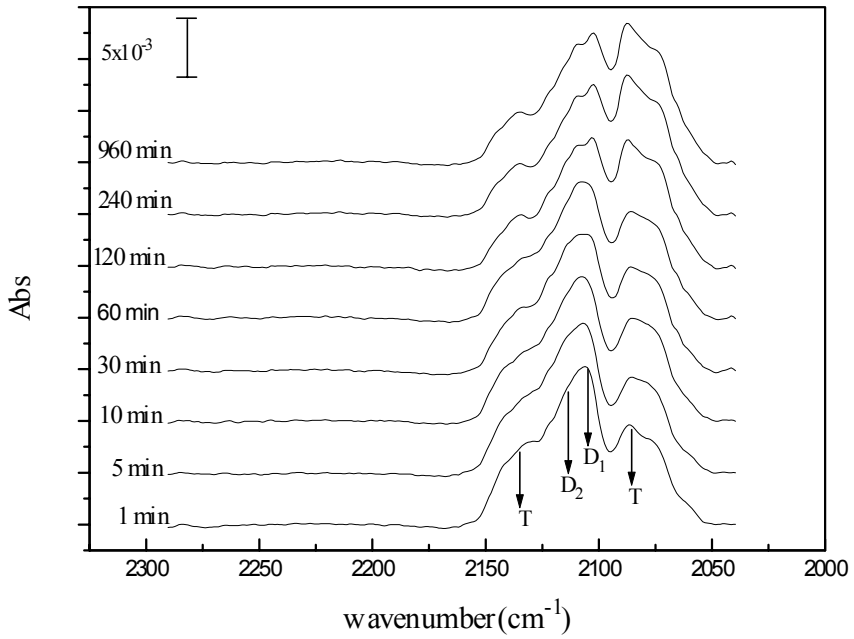


**Fig. 4.6.** Time dependant spectra for H-Si(100) surface immersed in 10 ppb $Cu^{2+}$ / 4.9% HF.

In this case the (100) facets are transformed into (111) facets indicating surface micro-roughness. It has been shown based on AFM that trace amounts of $Cu^{2+}$ form nanoscale deposits on the silicon surface along with localized pit formation.[12] The metal ions extract surface electrons from the silicon surface and deposit at certain active sites. The surface extraction of the silicon surface causes them to be oxidized, but as the substrate is immersed in HF these oxides are immediately etched. Thus trace amounts of metal contaminants in HF can cause severe damage to the silicon surface by changing its morphology. This phenomenon of metal deposition and localized etching results in increasing the surface roughness, which is easily detected by ATR spectroscopy.

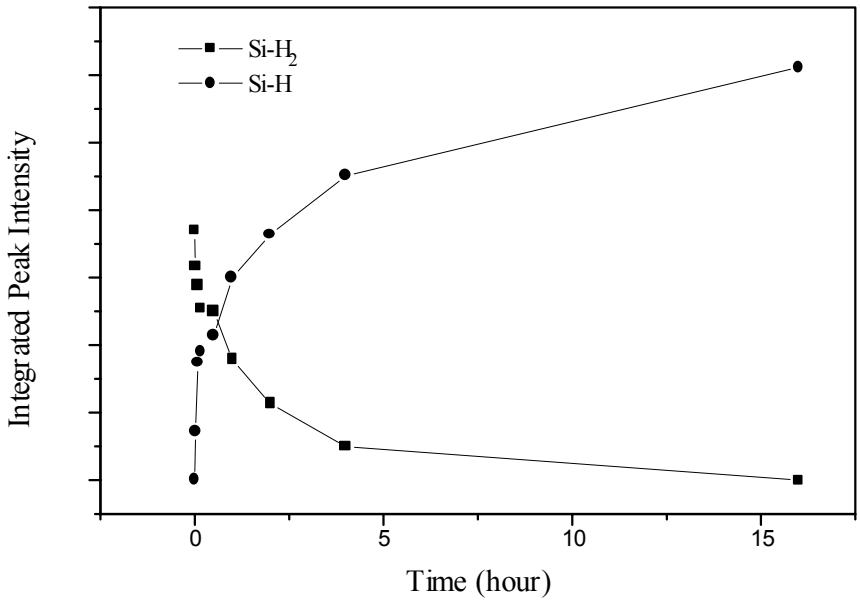


**Fig. 4.7.** Integrated peak intensity of H-Si(100) single in crystal in 10 ppb $Cu^{2+}$ / 4.9% HF.

### 4.3.1. Stability of H – terminated Si in UPW

The stability of H – terminated Si in different environments has been studied by a number of workers, but not much work has been carried out to investigate the early stages of oxidation of silicon surfaces when immersed in UPW. The silicon surface undergoes several changes in the early stages when it is immersed in UPW. These changes can be clearly seen by studying the different vibration modes of the H- terminated surface. This section deals with the initial stages of oxidation of H-Si(100) in UPW and $Cu^{2+}$ / UPW system. Fig. 4.8 shows the effect of immersing hydrogen-terminated silicon in UPW for different durations of time. Changes in the shape of the dihydride peaks can be observed after just 1 min indicating modification in the surface morphology The dihydride peaks represented by $D_1$ (2103.5 $cm^{-1}$) and $D_2$ (2114.6 $cm^{-1}$) are well defined as reflected by

their sharpness. This sharpness is possibly due to the etching of the (111) facets by the $OH^-$, which is present in UPW.

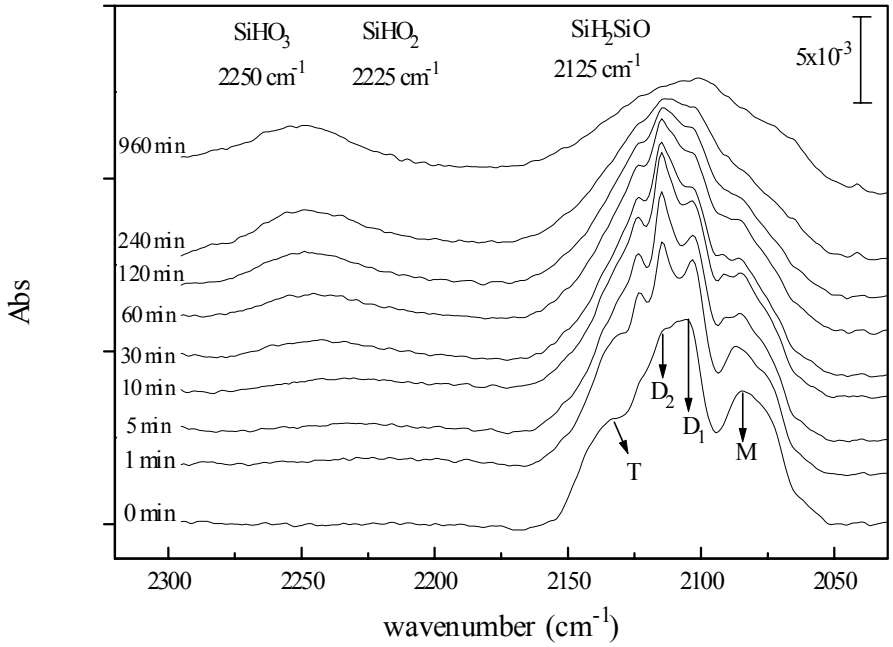


**Fig. 4.8.** ATR spectra of H-Si(100) immersed in UPW for different durations of time.

It is interesting to observe that the monohydride peak does not increase, but rather decreases with time as opposed to when immersed in HF. Niwano *et al.* observed this phenomenon but did not explain the reason for this occurrence.[13] They acquired their spectrum an hour after immersing the substrate in UPW, thus they did not account for the changes that the hydride region underwent between 0 and 1 hour. My study strives to throw light on the initial stages of the interaction of H-Si(100) with UPW. One of the reaction mechanisms based on STM (scanning tunneling microscopy) studies that was proposed is as follows,[14]

$$=SiH + H_2O \rightarrow =SiOH + H_2 \quad (4.1)$$

$$=Si\text{-}Si^{\delta+}\ OH^{\delta-} + H^+OH^- \rightarrow =SiH + =Si(OH)_2 \quad (4.2)$$

$$=SiOH + =Si(OH)_2 \rightarrow =Si\text{-}O\text{-}SiOH + H_2O \quad (4.3)$$

The first step is the formation of the silanol followed by the reaction of $OH^-$ with the silicon atoms present in the second layer (backbond) resulting in the formation of diols. The final step is the condensation of the silanols resulting in the formation of the oxide. My studies, on the other hand, have pointed to a different mechanism, which will be discussed later in this section.

Fig. 4.8 indicates a decrease in the monohydride and trihydride peak with immersion time, which can be explained by the fact that they are present at the step edges. These hydrides are quite unstable and susceptible to oxidation by $OH^-$ ions from water. Based on theoretical calculations it has been shown that hydroxylation of the hydrides is the first step involved in the oxidation process.[7,8] Fig. 4.8 also depicts the formation of an additional peak at 2125 $cm^{-1}$, which could correspond to the $SiH_2SiO$ configuration. Niwano *et al.* had observed a similar peak when exposing H-Si(100) to air for long durations of time.[9] The formation of $SiH_2SiO$ is known to occur due to the insertion of O atoms into the back bonds of the silicon lattice. The presence of an electronegative O atom shifts the dihydride peak position to a higher wave number. This O atom is considered to replace one of the Si back bonds thereby still leaving the surface H-Si(100). Another interesting observation is that the dihydride peaks namely $D_1$ and $D_2$ corresponding to the symmetric and asymmetric stretching peak position sharpen with time. The sharpness of these peaks indicates an increase in the number of dihydride structures. This can also be explained in terms of increase in the domain size. Domains

are structures having a similar bonding configuration in a particular plane. The presence of similar surface hydride species in a plane or more appropriately terraces results in a sharper peak.[15,16] This is especially true for the case of $D_2$, which increases in intensity with time and finally tapers of at the end of 60 min.

The initial stages of oxidation are depicted by the formation of broad peaks in the 2200 – 2250 $cm^{-1}$ region. The advent of peaks at 2225 and 2250 $cm^{-1}$ regions portray the progressive stages of oxidation. The broad peak at 2225 $cm^{-1}$ corresponding to the $SiH_2O_2$ structure appears at the end of 5 min. At 30 min, this peak disappears and a broad peak corresponding to $SiHO_3$ bonding configuration appears at 2250$cm^{-1}$ that increases with time. At 960 min the $SiHO_3$ peak decreases slightly in peak intensity. This decrease can be explained when one looks at the $SiO_2$ spectra of the H-Si(100) surface. Fig. 4.9 helps in explaining the different stages that are involved in the oxidation of H-Si(100) surfaces when exposed to UPW.

Fig. 4.9(a) represents an ideal H-Si(100) surface which has two dangling bonds that are capped with H atoms after etching with HF and two back bonded Si atoms present below the plane of the surface. Fig. 4.9(b) corresponds to the $SiH_2SiO$ configuration, which involves the insertion of an O atom in one of the back bonds, and 4.9(c) relates to the $SiH_2O_2$ state wherein both the back bonds are occupied by O atoms. The $SiH_2SiO$ peak is sharp, possibly due to the fact that the domain containing the dihydrides is not perturbed due to the presence of only one oxygen atom. On the other hand broad peaks are observed for $SiH_2O_2$ and $SiHO_3$ due to the increase in the number of oxygen atoms and also due to the amorphous nature of the oxide / suboxide that is formed. Fig. 4.9(d)

results when one of the H atoms is replaced by O atom and finally the surface silicon atom is bonded to only O atoms giving rise to the $SiO_4$ tetrahedron.

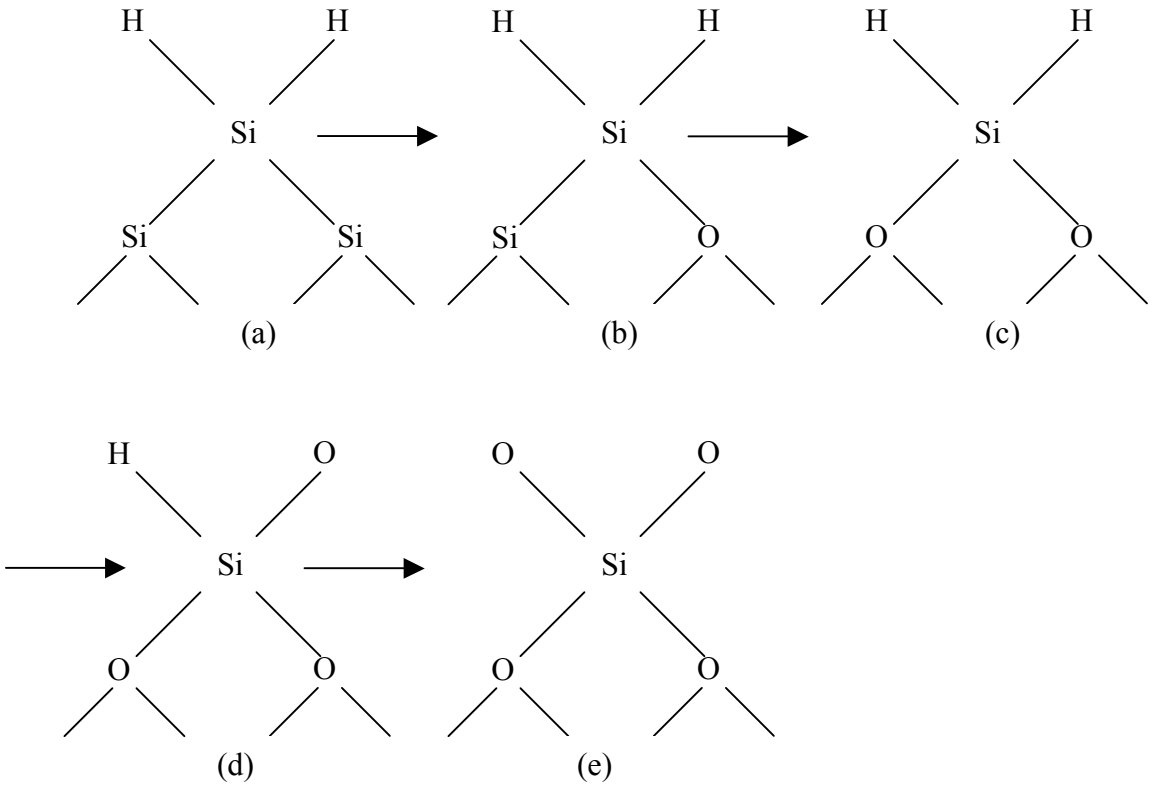


**Fig. 4.9.** Schematic of various bonding configurations which represents the different stages of oxidation of H-Si(100).

The silicon oxide spectral region as represented by Fig 4.10 has a lot of noise associated with it. The S/N ratio for the oxide spectral region is poor for the following reasons:

a) The Si phonon and multiphonon (lattice vibrations) absorption lie in the same frequency range as that of that the oxide.

b) The oxide that is formed is very thin and amorphous in nature (< 30 Å).

The broad peak at ~1200 $cm^{-1}$ corresponds to the longitudinal optical (LO) phonon mode of the $SiO_4$ tetrahedron. Generally the $SiO_2$ films are represented by the LO and TO phonon mode (transverse optical, ~1040 $cm^{-1}$), which arise due to the asymmetric stretching of the Si-O bond.[8] In this case, only the LO mode can be seen clearly at the end of 960 min, while the intensity of the TO mode is obscured by the noisy background.

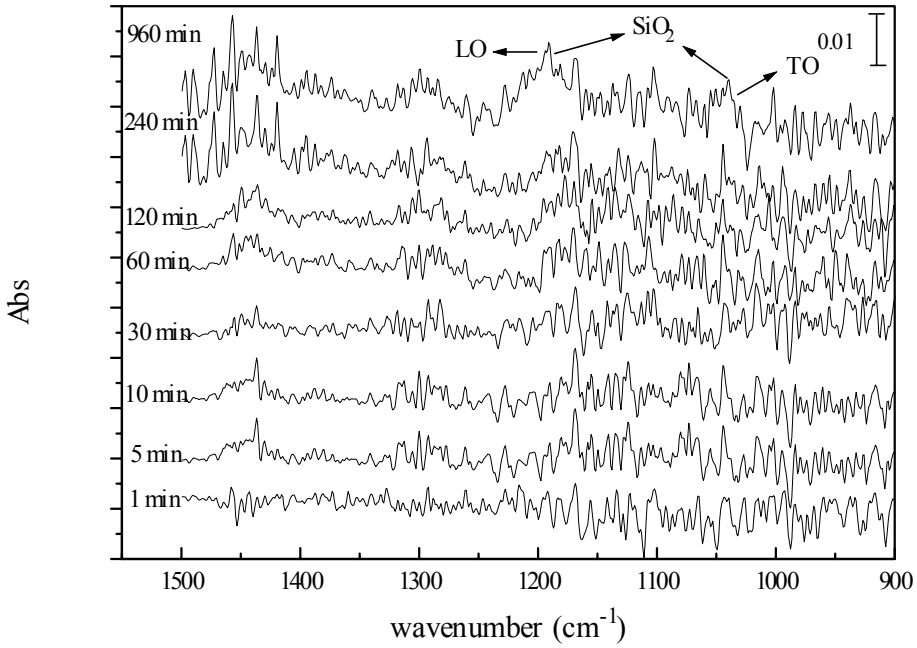


**Fig. 4.10.** $SiO_2$ spectral region of H-Si(100)

In this case, only the LO mode can be seen clearly at the end of 960 min, while the intensity of the TO mode is obscured by the noisy background. The appearance of

the LO peak coincides with the decrease in the $SiHO_3$ peak intensity indicating the progressive stages of oxidation of H-terminated Si surface as represented in Fig. 4.9. This indicates that the oxidation of the surface occurs in several stages each of which initially increases and then decreases giving rise to the next stage. A similar observation was made by Niwano *et al*. when they exposed H- terminated H-Si(100) to air for several days.[9] They did not look at the spectral region corresponding to the $SiO_2$ region but concluded that the surface was covered by a oxide film after long term exposure to air.

### 4.3.2. Stability of H – Terminated Si in $Cu^{2+}$ / UPW

Fig. 4.11 depicts the time dependant spectra of H-Si(100) surface immersed in 10 ppb $Cu^{2+}$ / UPW. There is a drastic change in the shapes of the hydride peaks in this system in a very short period of time. It is interesting to note that the dihydride peaks sharpen after 1 min immersion similar to the UPW case. This indicates that the surface termination is not disturbed during the initial stages of metal deposition. It seems like the surface is disrupted at the end of 5 min as indicated by the broadening of the hydride peak. The $SiH_2O_2$ (2225 $cm^{-1}$) configuration is less clear in any of the spectra, but one observes the advent of back bond oxide at the end of 5 min based on the broad peak at ~2250 $cm^{-1}$. With the passage of time, there is not only an increase in this peak but also a progressive shift to a higher wave number (2240 to 2260 $cm^{-1}$). At the end of 60 min the back bond oxide peak intensity starts to decrease and plateaus out at 960 min. The blue shift in the back bonded oxide is possibly due to the increase in the number of electronegative O atoms in the Si / $SiO_2$ inter-phase.

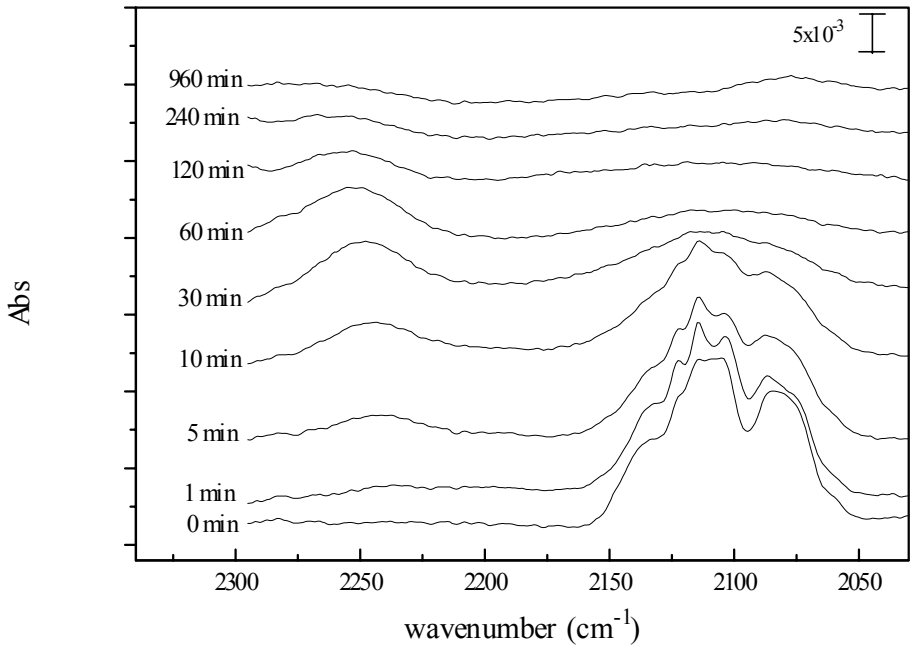


**Fig. 4.11.** Time dependent spectra of H-Si(100) immersed in 10ppb $Cu^{2+}$ UPW.

At the end of 120 min, the hydride peak disappears indicating the complete oxidation of the surface. In contrast, in the silicon substrate submerged in just UPW, a broad hydride peak remains even at the end of 960 min. Fig. 4.12 shows the normalized peak intensity with respect to time, based on which one can say that trace amounts of $Cu^{2+}$ greatly enhance the rate of oxidation. The rate of oxidation can be quantified based on either the appearance of an oxide peak or the disappearance of the hydride peak.

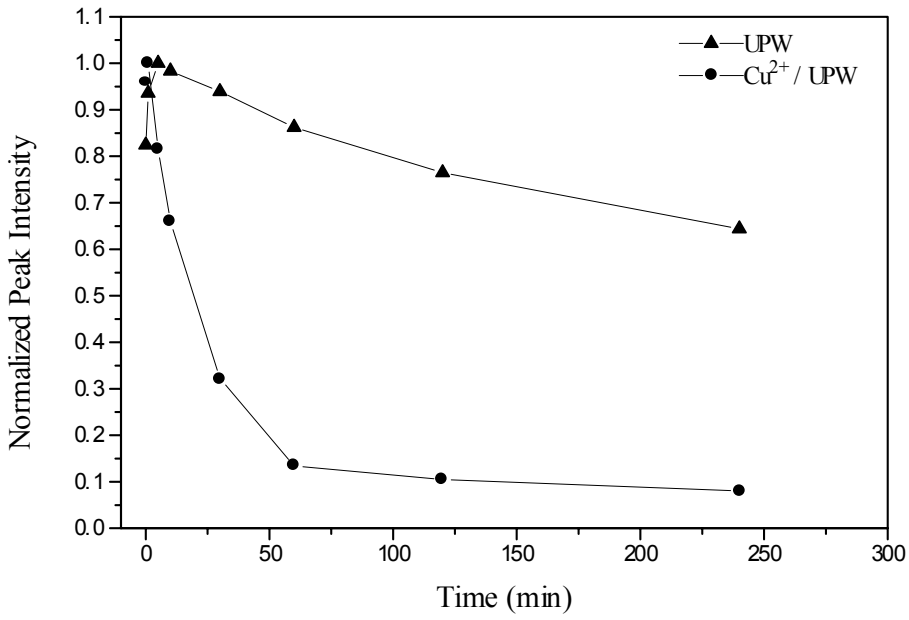


**Fig. 4.12.** Normalized peak intensity of H-Si(100) in UPW and 10 ppb $Cu^{2+}$ / UPW.

A clearer picture of the oxidation phenomenon can be obtained from Fig. 4.13 which relates to the $SiO_2$ spectral region wherein one observes the appearance of the LO and a TO mode as well at the end of just 30 min. The hydride peak, which disappears at the end of 120 min can be explained on observing the $SiO_2$ region depicted by Fig. 4.13. The $SiO_2$ peak increases with time and is clearly visible at the end of just 30 min. This deposition of trace amounts of metal impurities on the H- terminated surface that accelerate the formation of $SiO_x$ has been termed as metal induced oxidation.[17]

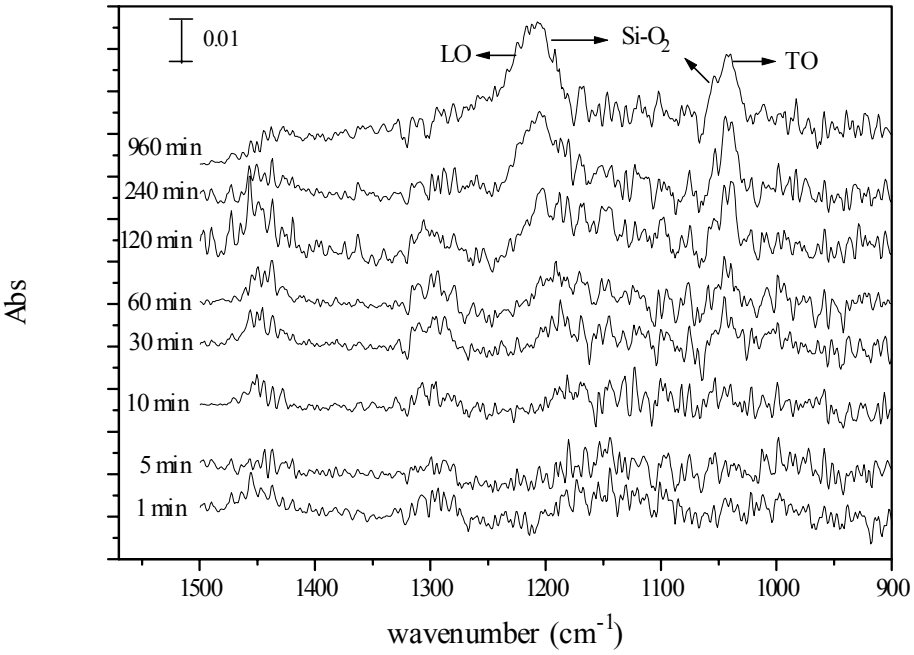


**Fig. 4.13.** $SiO_2$ spectral region of H-Si(100) in 10 ppb / UPW.

The deposition of noble metals like $Ag^+$, $Pt^{2+}$, $Cu^{2+}$ etc. on the H – terminated silicon surface will extract surface electrons from the silicon substrate resulting in its oxidation. In a HF system, due to the presence of $HF_2^-$ and HF etching immediately follows after the formation of this oxide. But in the case of UPW there are no comparable etching processes, thus resulting, in the increase of $SiO_2$ thickness. A plausible reaction for Cu deposition in UPW is

$$Si\text{-}H_x + Cu^{2+} + 2H_2O \rightarrow SiO_2 + Cu + xH+ \qquad (4.4)$$

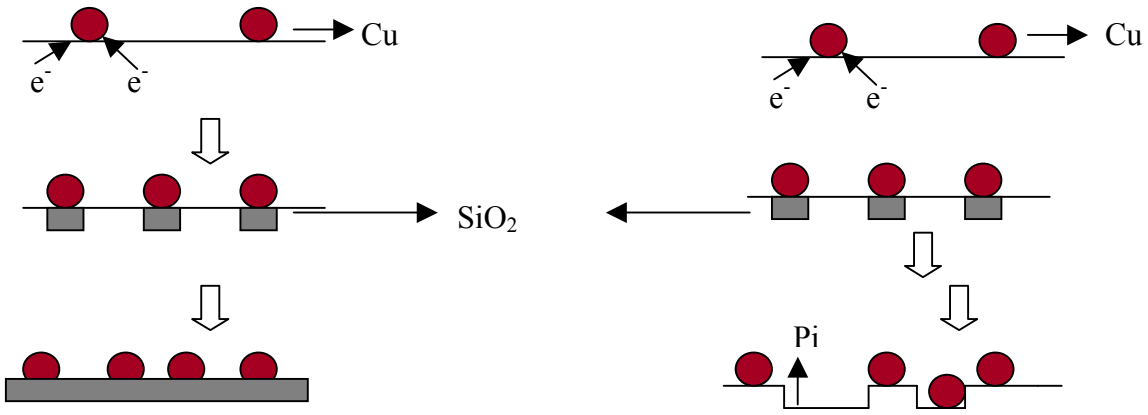


(a) (b)

**Fig. 4.14.** Schematic representation of the deposition of $Cu^{2+}$ on H-Si(100) in (a) UPW and (b) HF.

As can be seen in Fig. 4.14 when a H – terminated Si surface is immersed in a HF system containing trace amounts of $Cu^{2+}$, the deposition reaction proceeds with the oxidation of Si to $SiO_2$ which is instantly etched due to the presence of $HF_2^-$ and HFspecies. This etching of the oxide results in the formation of pits along with hillock formation due to Cu deposits as observed by AFM.[12] This is the reason for the observed surface roughening, as depicted in Fig. 4.5. On the other hand, in UPW, the formation of $SiO_2$ proceeds until the surface is completely covered with an oxide and thereby rendering the surface hydrophilic. According to Fig. 4.15 the back bonded peak intensity for both the systems increases with time, but at the end of 30 min the integrated peak intensity starts to drop for the Cu contaminated system. This initial rate of increase for the $Cu^{2+}$ / UPW

system is about 1.5 times that of pure UPW system. At the end of 30 min the peak intensity continues to rise for the substrate immersed in pure UPW, while it drops for the Cu containing system. This decrease is consistent with the increase in the $SiO_2$ peak intensity, which once again indicates a step-by-step mode of oxidation.

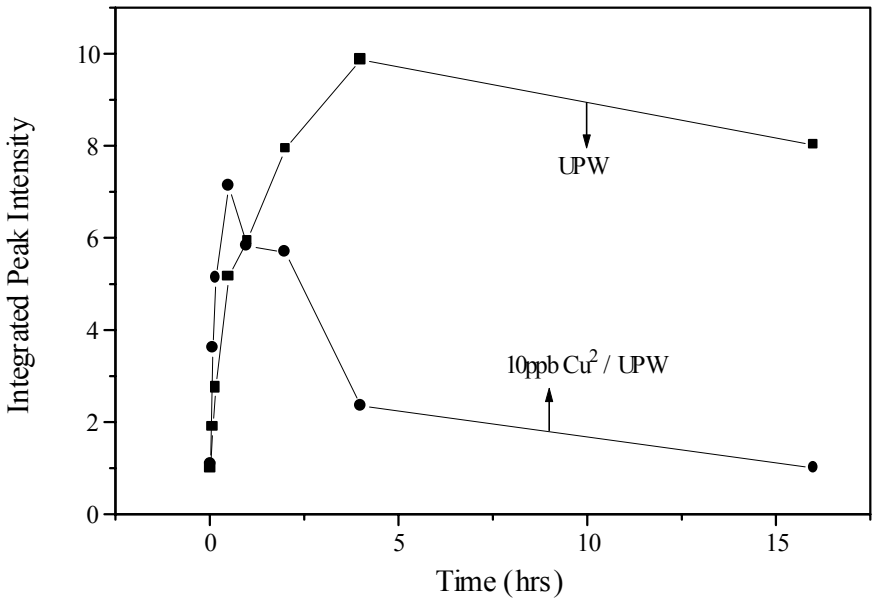


**Fig. 4.15.** Integrated peak intensity for the back bonded oxide ($SiHO_3$) for UPW and 10 ppb $Cu^{2+}$ / UPW.

Based on Fig. 4.12 one can make a semi-quantitative statement by saying that the substrate immersed in Cu contaminated system has a rate of oxidation which is at least 8 times greater than that of a pure one. The absorbance of the $SiO_2$ peak pertaining to the LO mode was compared with that obtained by the formation of a chemical oxide. The chemical oxide was obtained after immersing the H–Si(100) in a SC-1 solution. The absorbance value after 240 min was similar to that of the chemical oxide indicating that the oxide thickness must have been in the 30 - 50Å range.

### 4.3.3. Effect of Dissolved oxygen

This section deals with the effect of dissolved oxygen (DO) in UPW on H-Si(100) surfaces. UPW containing low amounts of DO is commonly used to rinse Si surfaces and to inhibit the early onset of oxidation. Thus it is important to understand the interaction of H - terminated Si surfaces in such a system. A few workers have already studied the effect of rinsing UPW with known dissolved oxygen on H - terminated Si surfaces. Morita *et al*. were one of the first to study the effect of immersing Si(100) in UPW containing 9 ppm of DO. They measured the thickness of the native oxide that grew with immersion time and concluded that the oxide growth reached a saturation point after about 165 hrs.[2] Kanaya *et al.* studied the effect of immersing H-Si(100) in UPW containing 5 ppb of DO.[18] They used ATR spectroscopy to study the different vibrational modes for the various hydrides and observed the sharpening of the dihydride peaks between 1 – 5 hrs followed by the formation of (111) and (110) facets indicating surface roughening. They go on to show that the dihydride peak was retained even after 45 hrs of rinsing. This section deals with a comparative study that was undertaken in which the Si substrate was immersed in two systems with varying amounts of dissolved oxygen. Fig. 4.8 depicts the spectra for H-Si(100) in UPW exposed to the ambient atmosphere and was found to contain 8 ppm DO based on the DO probe mentioned in the experimental section. This value was found to tally with those obtained by theoretical calculations based on Henry's Law.

Henry's law states: $P_b = X_b \times K_b$

$P_b$ is the partial pressure of species b in the atmosphere

$X_b$ is the mole fraction of species b in solution

$K_b$ is the Henry's law constant

The oxygen content in the atmosphere can be considered to 21% assuming the atmospheric pressure to be 1atm (760torr).

$\Rightarrow P_{O_2} = 159.6$ torr

Henry's $K_{O_2} = 3.3$ e-7 (or 0.00000033) torr [19]

$\Rightarrow X_{O_2} = n_{O_2} / [n_{O_2} + n_{H_2O}] = n_{O_2} / n_{H_2O}$ ($n_{O_2} << n_{H_2O}$)

$\Rightarrow n_{O_2} / n_{H_2O} = P_{O_2} / K_{O_2} = 159.6$ torr / 3.3 e-7 torr

$n_{H_2O} = 55.5$ moles for 1 L of solution

$\Rightarrow n_{O_2} = 2.68$ e-4 moles (in 1 liter) = 8.57 mg / L. Therefore the concentration of DO amounts to ~8.57 ppm under ambient conditions which is fairly close to the experimental value of 8ppm.

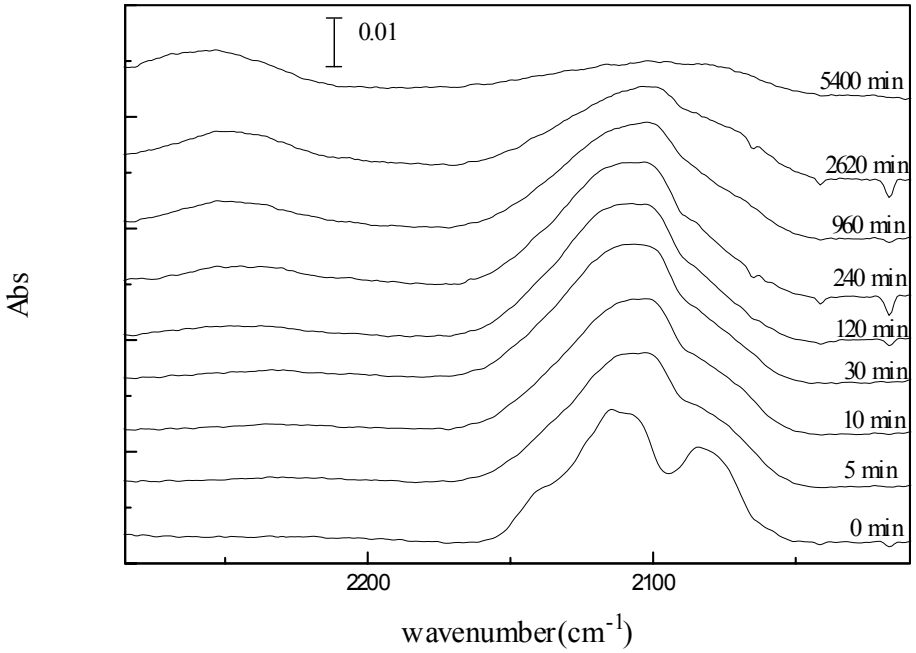


**Fig. 4.16.** H-Si(100) immersed in UPW bubbled with $N_2$ ( DO content = 2.5 ppm).

Comparison of Fig. 4.16 with Fig. 4.8 shows marked difference in the evolution of the two spectra. As mentioned in the experimental section, the beaker containing UPW was bubbled with $N_2$ to displace the DO present. The Si substrate immersed in UPW containing 2.5 ppm DO does not show any of the sharpening of the dihydrides that is observed in its 8 ppm counterpart. In fact the hydride region is featureless indicating that a totally different mechanism is in effect.

The presence of a broad hydride region in Fig. 4.16 indicates that the hydrides present in the surface have small domain sizes and are thereby not able to interact with each other to give rise to sharp features.[16] One can definitely say that the rate of oxidation is retarded in a system containing lower amounts of DO. The back bond oxide peak in the 2200 – 2250 $cm^{-1}$ region appears only after the end of 30 min as compared to 5 min in the 8 ppm case. This is made apparent when one looks at Fig. 4.17, which compares the relative peak area of the hydride peak under the two different conditions. There is a decrease in peak intensity in the system containing 8 ppm of DO, while in the 2.5 ppm case there seems to be some sort of equilibration between 30 – 120 min after which the peak intensity tends to drop gradually. At the end of 960 min more than 70% of the hydride peak is retained when the silicon surface is immersed in UPW containing 2.5 ppm. Under similar conditions only about 40% of the hydride peak is observed when the substrate is immersed in UPW containing 8 ppm DO. It is worthwhile to mention that when the Si surface that has been immersed in UPW containing 2.5 ppm retains about 55% of the hydride peak area even after 47 hrs. The steady increase in the $SiHO_3$ back bond peak indicates that the surface is not completely covered with an oxide layer if one assumes the step wise oxidation mechanism as discussed in the previous sections.

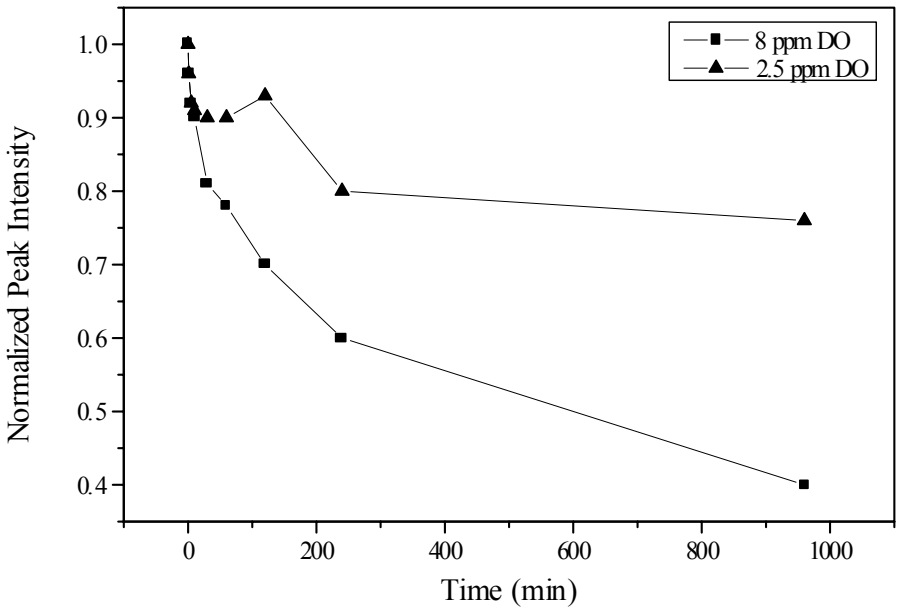


**Fig. 4.17.** Comparison of relative peak area for H-Si(100) in different DO concentrations.

It may be concluded that the surface is not completely covered with an oxide layer. It thus becomes very clear that removal of dissolved oxygen from the system is essential to maintain stable H-Si(100) surfaces.

Another interesting phenomenon that is observed when the Si substrate is immersed in UPW containing 2.5 ppm DO is the shape of the hydride peaks. The normal features of the dihydride peak are no longer observed from the very first minute. One can only observe a featureless hydride region when $N_2$ bubbling is used to drive out the DO from the system as mentioned earlier. To verify the impact of $N_2$ bubbling, another experiment was carried out where the Si substrate was immersed in UPW containing 2.5 ppm, but this time instead of bubbling the system it was covered by $N_2$ blanket. It is interesting to note that one does observe the characteristic features of the dihydride peak

in this case as seen in Fig. 4.18. The formation of a well-defined dihydride peak is observed as in the case of the UPW containing 8 ppm DO. The back bond oxide feature appears only at the end of 30 min and is similar to the case when the system is bubbled with $N_2$. Thus, the mere act of bubbling the system to drive out the DO seems to be causing some sort of perturbation and thereby inhibiting the normal etching process on the silicon surface. In order to explain the formation of featureless hydride peaks, one needs to look at the cause of formation of these peak shapes observed upon immersion in UPW.

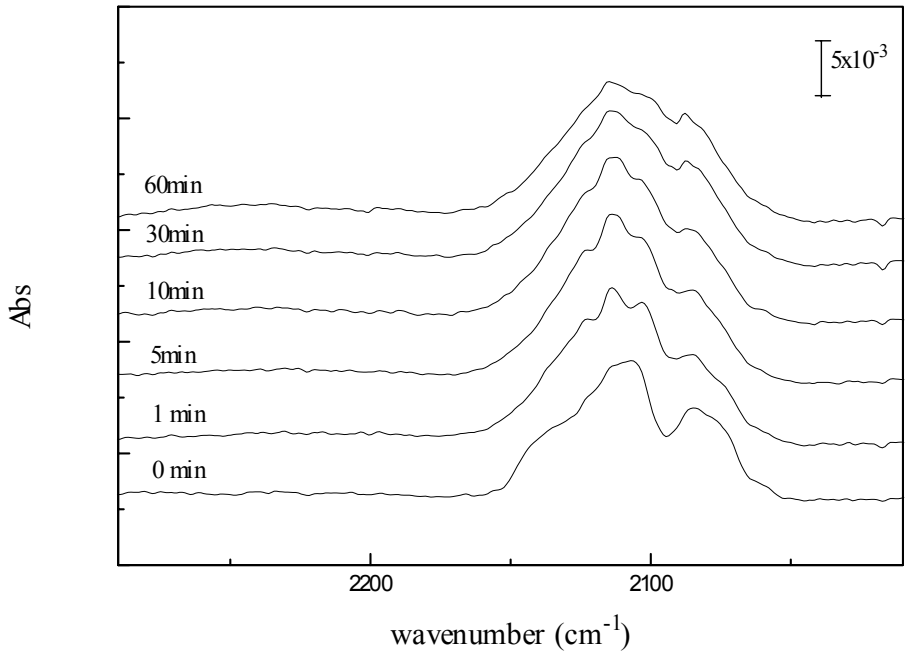


**Fig. 4.18.** H-Si(100) immersed in UPW 2.5 ppm DO content w / o $N_2$ bubbling.

Earlier studies have shown that the silicon surface is etched in UPW by the $OH^-$ ions.[7,20] Thus, on bubbling the system it is quite possible that the pH of the system was altered. To verify this, the pH of the system was measured during the course of the

bubbling experiment and found that it remained unchanged. Once it was ascertained that the pH did not change by the act of bubbling the system, the formation of featureless peaks being a chemical phenomenon could be ruled out. It seems like the formation of multi-facets are more of a physical phenomenon, namely the interaction of bubbles with the H-Si(100) silicon surface. Localized etching by $OH^-$ causes the formation of sharp dihydride features when the substrate is immersed in UPW without $N_2$ bubbling. This seems to indicate that the act of bubbling causes random etching leading to the formation of a multifaceted structure thereby giving rise to a featureless hydride peak.

In summary, it has been shown that metallic ions and the presence of dissolved oxygen in UPW are the root causes for oxidizing the H-Si(100) silicon surface on immersing it in UPW. In order to maintain stable silicon surfaces, it is imperative to maintain an environment that is well controlled and devoid of trace metallic contaminants. The results generated by the experiments have important ramifications towards the semiconductor industry since silicon wafer surface needs to be stable and defect free between the different processes involved in the fabrication of IC devices.

## 4.4 Chapter References


1. T. Sunada, T. Yasaka, M. Takakura, T. Sugiyama, S. Miyazaki and M. Hirose*, J. Appl. Phys.*, **29**, 2408 (1990).
2. M. Morita, T. Ohmi, E. Hasegawa and A. Teramoto, *Jpn. J. Appl. Phys*. **29**, 2392 (1990).

3. A. Y. Vul, T. L. Makarova, V. Y. Osipoes, Y. S. Zinchik and S. K. Boltsov, *Sov. Phys. Semicond*., **26**, 62 (1992).

4. E. P. Boonekamp, J. J. Kelly, J. Vande Van and A. H. M. Sondag, *J. Appl. Phys*., **75**, 8121 (1994).

5. M. Niwano, T. Miura and N. Miyamoto, *J. Electrochem. Soc*., **145**, 659 (1998).

6. M. K. Weldon, B. B. Stefanov, K. Raghavachari and Y. J. Chabal*, Phys. Rev. Lett*., **79**, 285 (1997).

7. T. Tada and R. Yoshimura, *Phys. Lett. A*, **220**, 224 (1996).

8. Y. J. Chabal, Fundamental Aspects of Silicon Oxidation, Springer Series, New York, 2001.

9. M. Niwano, J. Kageyama, K. Kinashi, J. Sawahata and N. Miyamoto*, Surf. Sci. Lett*., **301**, 245 (1994).

10. H. N. Waltenburg and J.T. Yates, *Chem. Rev.*, **95**, 1589 (1995).

11. G. Willeke and K. Kellermann, *Semicond. Sci. Technol*., **11**, 415 (1996).

12. O. M. R. Chyan, J. J. Chen, H. Y. Chien, L. Hall and J. Sees, *J. Electrochem. Soc*, **143**, 92 (1996).

13. M. Niwano*, Surf. Sci.,* **427**, 199 (1999).

14. G.J. Pietch, U. Köhler and M. Henzler, *Chem. Phys. Lett*., **197**, 346 (1992).

15. P. Jakob, Y. J. Chabal and K. Raghavachari, *Chem. Phys. Lett*., **187**, 325 (1991).

16. P. Jakob, Y. J. Chabal, K. Raghavachari and S.B. Christman*, Phys. Rev. B.,* **47**, 6840 (1993).

17. J. S. Kim, H. Morita, J. D. Joo and T. Ohmi, *J. Electrochem. Soc*., **144**, 3275 (1997).

18. H. Kanaya, K. Usuda and K. Yamada*, Appl. Phys. Lett*. **67**, 682 (1995).

19. R. C. Weast, W. H. Beyer and M. J. Astle, *CRC Handbook of Chemistry and Physics*, CRC Press: Boca Raton (1988).

20. S. Watanabe and Y. Sugita, *Appl. Surf. Sci*., **107**, 90 (1996).

# CHAPTER 5

# CONCLUSION

Hydrogen terminated silicon surfaces were successfully utilized to develop sensors to detect metallic contaminants and the interaction of such surfaces under different environments was studied.

Potentiometric detection of trace levels of metallic contaminants using a silicon-based sensor in hydrofluoric acid with respect to two non-contaminating reference electrode systems was discussed in chapter 2. In the first case, conductive diamond was used as a reference electrode. Cyclic voltammetry and open circuit potential experiments demonstrated the feasibility of conductive diamond to be used as a quasi-reference electrode. In the second case, a dual silicon electrode system was used with one of the silicon-based electrodes protected with an anion permeable membrane behaving as the quasi reference electrode. Though both systems can function well as a suitable reference system, the dual silicon electrode design showed greater compatibility for the on-line detection of metallic impurities in HF etching baths. The silicon-based sensor assembly was able to detect parts- per-trillion to parts-per-billion levels of metal ion impurities in HF.

A novel method for the detection of $Ni^{2+}$utilizing attenuated total reflection (ATR) technique was discussed in chapter 3. The nickel infrared sensor was prepared on a silicon ATR crystal uniformly coated by a 1.5 micron Nafion film embedded with dimethylglyoxime (DMG) probe molecules. The detection of $Ni^{2+}$ was based on the

appearance of a unique infrared absorption peak at 1572 $cm^{-1}$ that corresponds to the C=N stretching mode in the nickel dimethylglyoximate, $Ni(DMG)_2$, complex. The suitable operational pH range for the nickel infrared sensor was between 6-8. High alkalinity in the sample solution causes excess leaching of $Ni(DMG)_2$. Interference studies revealed that $Cu^{2+}$ could compete with $Ni^{2+}$ for the DMG binding sites in the Nafion matrix. However, $Cu(DMG)_2$ complex exhibits C=N infrared absorption peak at 1560 $cm^{-1}$. The detection limit of the nickel infrared sensor was 1 ppm in the sample solution of pH=8.

Chapter 4 dealt with the interaction of hydrogen terminated Si(100) surfaces under different environments. ATR – FTIR spectroscopy was used to study the changes that the hydride mode underwent when subjected to different environments. The presence of trace amounts of $Cu^{2+}$ in HF solutions was found to roughen the silicon surface as observed by ATR IR spectroscopy. The initial stages of oxidation in UPW and $Cu^{2+}$ / UPW was studied. Trace amounts of $Cu^{2+}$ were found to drastically increase the rate of oxidation, while the rate of oxidation was found to be retarded on removing dissolved oxygen that was present in UPW.

# REFERENCES


Allongue, P., Costa-Klieng, V., and Gerischer, H., *Electrochim. Acta,* 40, 1353 (1995).

Allongue, P., Costa-Klieng, V., and Gerischer, H., *J. Electrochem. Soc.,* **140**, 1018 (1993).

Angus, J. C.; Hayman, C. C., *Science*, **241**, 913 (1988).

Baldwin, R. P., Christensen, J. K., and Kruger, L., *Anal. Chem.*, **58**, 1790 (1986).

Bergerson, W. F., Mulder, J. A., Hsung, R. P., and Zhu, X. Y., *J. Am. Chem. Soc*., **121**, 454 (1999).

Bigotto, A., Galasso, V., De Alti, G., *Spectrochim. Acta.*, **27A**, 1659 (1971).

Bigotto, A., Costa, G., Galasso, V., De Alti, G., *Spectrochimi. Acta.***, 26A**, 1939 (1970).

Blinc, R., and Hadzi, D., *J. Chem. Soc.,* 4536 (1958).

Boonekamp, E. P., Kelly, J. J., Vande Van, J., and Sondag, A. H. M., *J. Appl. Phys*., **75**, 8121 (1994).

Brandrup, J., Imergut, E. H., Grulke, E. A., Handbook of Polymers. Wiley – Interscience Publication: N.Y., 1998.

Burrows, V. A., Chabal, Y. J., Higashi, G. S., Raghavachari, K., and Christman, S. B., *Appl. Phys. Lett*., **53**, 998, (1988).

Chabal, Y. J., Fundamental Aspects of Silicon Oxidation, Springer Series, New York, 2001.

Chabal, Y. J., Higashi, G. S., Raghavachari, K., and. Burrows, V. A., *J. Vac. Sci. Technol.*, **A7**, 2104, (1989).

Chen, J. J., Xu, F., Ponnuswamy, T., Chan, R., Wu, J. J., Prasad, A., and Chyan, O., *Recent Res. Devel. Applied Spectroscopy*, **3**, 81 (2000).

Chen, J., and Gardella, J. A., *Appl. Spectrosc.*, **52**, 361 (1998).

Chyan, O. M. R., Chen, J. J., and Chien, H. Y., Sees, J. A., and Hall, L., *J. Electrochem. Soc.*, **143**, 92 (1996).

Chyan, O. M. R., Chen, J. J., and Wu, J. J., *Appl. Spectrosc.*, **51**, 1901 (1997).

Chyan, O. M. R., Chen, J. J., Chien, H. Y., Hall, L. H., Sees J. A., *J. Electrochem. Soc*, **143**, 92 (1996).

Chyan, O., Chen, J. J., Chein, H. Y., Wu, J. J., Liu, M., Sees, J., and Hall, L., *J. Electrochem* Soc., **143**, L235 (1996).

Chyan, O., Chen, J. J., Chen, L., Xu, F., *J. Electrochem* Soc., **144**, L18 (1997).

Chyan, O., Chen, J. J., Chein, H. Y., Sees, J., and Hall, L., J. *Electrochem* Soc., **143**, 92, (1996).

Chyan, O., Chen, J. J., Xu, F., Sees, J., and Hall, L., *Analyst,* **125**, 175, (2000).

Chyan, O., Chen, J.J., Xu, F., and Wu, J. J., *Anal. Chem.*, **69**, 2434 (1997).

Cotton, F. A., and Murillo, C., Advanced Inorganic Chemistry, John Wiley & Sons (1999).

Covington, A. K., *Ion–Selective Electrode Methodology*, Vol. 1, CRC Press Inc., Florida (1979).

Dean, J. A., Lange's Handbook of Chemistry, 13th Edition, McGraw Hill Inc. (1972).

DeGrandpre, M. D., Burgess, L. W., White, P. L., and Goldman, D. S., *Anal. Chem*., **62**, 2012 (1990).

Falk, M., *Can. J. Chem.*, **58**, 1495 (1980).

Gorostiza, P., Diaz, R., Servat, J., and. Sanz, F., J. Electrochem. Soc., **144**, 909 (1997).

*Handbook of Semiconductor Wafer Cleaning Technology*, W. Kern ed.; Noyes Publications, Park Ridge, New Jersey, (1993).

Harrick, N. J., Internal Reflection Spectroscopy, Interscience Publishers: N.Y. (1967).

Higashi, G. S., Chabal, Y. J., Trucks, G. W., and Raghavachari, K., *Appl. Phys. Lett*., **56**, 656, (1990).

Homma, T., Wade, C. P., and Chidsey, C. E. D., *J. Phys. Chem. B,* **102**, 7919 (1999).

Ives, D. J. G., Janz, G. J., *Reference Electrodes*, Academic Press Inc. N.Y. (1961).

Jaeger, R. C., Introduction to Microelectronic Fabrication, Addison-Wesley Publishing Company Inc., U.S.A., 1988.

Jakob, P., Chabal, Y. J., Raghavachari, K., and Christman, S. B., *Phys. Rev. B.,* **47**, 6840 (1993).

Jakob, P., Chabal, Y. J., Raghavachari, K., *Chem. Phys. Lett*., **187**, 325 (1991).

Jeon, J. S., Sperline, R. P., and Raghavan, S., *Appl. Spectrosc.*, **46**, 1644 (1992).

Kanaya, H., Usuda, K., and Yamada, K., *Appl. Phys. Lett*. **67**, 682 (1995).

Kern, W., Handbook of Semiconductor Wafer Cleaning Technology, Noyes Publications, Park Ridge, NJ (1993).

Kern, W., *J. Electrochem. Soc.*, **137**, 1887 (1990).

Kern, W., *RCA Review*, Part I: **31**, 207 (1970). ; Part II: **31**, 234 (1970). ; Part III: **32**, 64 (171).

Kikyuama, H., Miki, N., Saka, K., Takano, J., Kawanabe, I., Miyashita, M., Ohmi, T., *IEEE Trans. Semicond. Manufact.,* **4**, 26 (1991).

Kim, J. S., Morita, H., Joo, J. D., and Ohmi, T., *J. Electrochem. Soc*., **144**, 3275 (1997).

Kniffin, M. L., Beerling, T. E., and. Helms, C. R., *J. Electrochem* Soc., **139**, 1195 (1992).

Lamontagne, M. C., Parthum, K. A., Rudolph Seitz, W., Tomellini, S.A., *Appl. Spectrosc.*, **48**, 1539 (1994).

Lee, H. J., Hong, U. S., Lee, D. K., Shin, J. H., Nam, H., and Cha, G. S., *Anal. Chem*., **70**, 3377 (1998)

Lester, A., *Semiconductor International*, **25**, 40 (2002).

Lewis, C. L., Ott, W. L., Analytical Chemistry of Nickel, Pergamon Press, Oxford, (1970).

Lewis, C. L., Ott, W. L., and Sine, N. M., Analysis of Nickel, Pergamon Press Inc., Oxford, (1966).

Li, L. F., Totir, D., Miller, B., Chottiner, G., Argoitia, A., Angus, J. C., and Scherson, D. A., *J. Am. Chem. Soc.,* **119**, 7875 (1997).

Liu, H., and Hamers, R. J., *J. Am. Chem. Soc.*, 119, 7593 (1997).

Liu, M.R., Liu, D. J., and Sun, A. L., *Analyst*, **117**, 1335 (1992).

Maurel, V. B., Vallat, C., and Goffinet, D., Appl. *Spectrosc.,* **49**, 556 (1995).

Maurel, V. B., Vallat, C., and Goffinet. D., *Appl. Spectrosc.*, **49**, 563 (1995).

Miller, J. B., and Brandes, G. R., *J. Appl. Phys.,* **82**, 4538 (1997).

Mirabella, F. M., Harrick, N. J., Internal Refletion Spectroscopy: Review and Supplement, Harrick Scientific Corporation, N. Y. (1985).

Morita, M., Ohmi, T., Hasegawa, E., and Teramoto, A., *Jpn. J. Appl. Phys*. **29**, 2392 (1990).

Mouche, L., Tardif, F., and Derrien, J., *J. Electrochem. Soc*., **142**, 2395 (1995).

Nagahara, L. A., Ohmori, T., Hashimoto, K., and Fujishima, A., *J. Vac. Sci. Technol*., **A11 (4)**, 763 (1993).

Nagy, K., Eine, K., Syverud, K., and Aune, O., J. *Electrochem* Soc., **144**, L1 (1997).

Niwano, M., Kageyama, J., Kinashi, K., Sawahata, J., and Miyamoto, N., *Surf. Sci. Lett*., **301**, 245 (1994).

Niwano, M., Miuara, T., and Miyamoto, N., *J. Electrochem. Soc.*, **145**, 659 (1998).

Niwano, M., Miura, T., and Miyamoto, N., *J. Electrochem. Soc*., **145**, 659 (1998).

Niwano*,* M., *Surf. Sci.,* **427**, 199 (1999).

Norga, G. J., Platero, M., Black, K. A., Reddy, A. J., Michel, J., and. Kimerling, L. C., *J. Electrochem. Soc.*, **144**, 3323 (1997).

Nriagu, J. O., and Niebor, E., Chromium in the Natural and Human environment. A wiley - Interscience publication, N.Y. (1988).

Nriagu, J. O., and Sprague, J. B., Cadmium in the Aquatic Environment. A wiley – Interscience publication, N.Y. (1987).

Ohmi, T., Imaoka, T., Sugiyama, I., and Kesuka, T., *J. Electrochem* Soc., **139**, 3317 (1992)

Palinko, I., Torok, B., Surya, G. K., and Olah, G. A., *Appl. Catal. B.,* **174**, 147 (1998).

Pan, L.S.; Kania, D.R., Eds., *Diamond: Electronic Properties and Applications*, Kluwer Academic Publishers, Boston, 1995.

Panja, P. K., Bala, S., Pal, C., and Ghosh, P. N., *J. Mol. Str.* 249, 277 (1991).

Peshkova, V. M., and Savastina, V. M., Analytical Chemistry of Nickel. Israel Program for Sceintific Translations, (1967).

Pietch, G. J., Köhler, U., and Henzler, M., *Chem. Phys. Lett*., **197**, 346 (1992).

Quezado, S., and Kwak, J. C. T., and Falk, M., *Can. J. Chem.*, **62**, 958 (1984).

Raghavachari, K., Higashi, G. S., Chabal, Y. J., and Trucks, G. W., Mat. Res. Soc. Symp. Proc., **315**, 437 (1993).

Reagan, F., Meaney, M., Vos, J. G. MacCraith, B. D., Walsh, J.E., Anal*. Chim. Acta.,* **334**, 85 (1996).

Riley, D., and Carbonell, R., *Proc. of The Institute of Enviromental Sciences Ann. Tech, Mtg.,* pp 224-228, New Orleans, LA (1990).

Sawyer, D. T., and Roberts, J. L., *Experimental Electrochemistry for Chemists*, Wiley-Interscience Publication, NY (1974).

Sawyer, D. T., Sobkowiak, A., Roberts, J. L., *Electrochemistry for Chemists*, Wiley-Interscience Publication, NY (1995).

Skoog, D. A., West, D. M., and Holler, F. J., Fundamentals of Analytical Chemistry, Seventh Edition, FL. (1997).

Spears, K. E., Dismukes, E. J. P., Eds.; *Synthetic Diamond: Emerging CVD science and Technology*; John Wiley and Sons: New York, 1994.

Sunada, T., Yasaka, T., Takakura, M., Sugiyama, T., Miyazaki, S., and Hirose, M., *J. Appl. Phys.*, **29**, 2408 (1990).

Suzuki, H., Shiroishi, H., Sasaki, S., and Karube, I., *Anal. Chem*., **71**, 5069 (1999).

Tada, T., and Yoshimura, R., *Phys. Lett. A*, **220**, 224 (1996).

Teerlinck, I., Mertens, P. W., Schimdt, H. F., Meurius, M., and Heyns, M. M., J. Electrochem. Soc., **143**, 3323 (1996).

Toei, K., Motomizu, S., and Kuse, S., *Anal. Chim. Acta*., **75**, 323 (1975).

Verhaverbeke, S., H. Bendar, H., Meuris, M., Mertens, P. W., Schmidt, H. F., and Heyns, M. M., *Mat. Res. Soc. Symp. Proc*., **315**, 457 (1993).

*VLSI Technology*; S.M. Sze ed.; McGraw Hill: New York, 1988.

Vul, A. Y., Makarova, T. L., Osipoes, V. Y., Zinchik, Y. S., and Boltsov, S. K., *Sov. Phys. Semicond*., **26**, 62 (1992).

Waltenburg, H. N., and Yates, J. T., *Chem. Rev*., **95**, 1589 (1995).

Wang, J., Nascimento, V. B., Lu, J., Park, D. S., and Agnes, L., *Electroanalysis,* **8**, 635 (1996).

Wang, J., Pamidi, P. V. A., Nascimento, V. B., and Agnes, L., *Electroanalysis*, **9**, 689 (1997).

Wang, J., Swain, G. M., Tachibana, T., and Kobashi, K., *Electrochem. Solid State Lett.*, **3**, 286(2000)

Watanabe, S., and Sugita, Y., *Appl. Surf. Sci*., **107**, 90 (1996).

Weast, R. C., Beyer, W. H., Astle, M. J., CRC Handbook of Chemistry and Physics, CRC Press: Boca Raton, 1988.

Weigner, C. H., *Polymer,* **20**, 371 (1979).

Weldon, M. K., Stefanov, B. B., Raghavachari, K., and Chabal, Y. J., *Phys. Rev. Lett*., **79**, 285 (1997).

Willeke, G., and Kellermann, K., *Semicond. Sci. Technol*., **11**, 415 (1996)

Xu, J., Granger, M. C., Chen, Q., Strojek, J. W., Lister, T. E., Swain, G. W., *Anal. Chem*., **69**, 591A (1997).

Yang, L. and Saavedra, S. *Anal. Chem*., **67**, 1307 (1995).

Yoon, H. J., Shin, J. H., Lee, S. D., Nam, H., Cha, G. S., Strong, T. D., Brown, R. B., *Sensors and Actuators B*, **64**, 8, (2000).

Zant, P. V., Microchip Fabrication: A Practical Guide to Semiconductor Processing, McGraw – Hill (1997).

Zen, J. M., and. Lee, M. L., *Anal. Chem*, **65**, 3238 (1993).